NANO · MICRO small
www.small-journal.com

Solid-State Electrolytes for Rechargeable Magnesium-Ion Batteries: From Structure to Mechanism

Miao Guo, Chongyang Yuan, Tengfei Zhang, and Xuebin Yu**

Rechargeable magnesium (Mg)-ion batteries have received growing attention as a next-generation battery system owing to their advantages of sufficient reserves, lower cost, better safety, and higher volumetric energy density than lithium-ion batteries. However, Mg as an anode can be easily passivated during charging/discharging by most common solvents, which are inconducive for magnesium deposition/stripping. Based on this, the development of Mg-ion solid-state electrolytes in the last decades led to the formulization of several concepts beyond previously reported designs. These exciting studies have once again sparked an interest in all-solid-state magnesium-ion batteries. In this review, Mg solid-state electrolytes, including inorganic (oxides, hydrides, and chalcogenides) and organic (metal-organic frameworks and polymers) materials are classified and summarized in detail. Moreover, the structural characteristics and the migration mechanism of Mg^{2+} ions are also discussed with a focus on pending questions and future prospects.

1. Introduction

With the increasing environmental problems and the emphasis on the energy crisis, renewable and clean energy (wind, solar, and hydrogen power) is in highly considered and appreciated. However, new energy resources are intermittent and may not meet practical applications. From a technological perspective, energy storage technology combined with clean energy will be crucial pillars of a successful future energy strategy. As an efficient energy storage device, lithium-ion batteries (LIBs) have low redox potential and high energy density. After decades of significant developments, LIBs have become a successful commercial energy storage technology and play essential roles in a multitude of applications ranging from consumer electronics and electric vehicles to aerospace products.[1–6] However, the high cost of the limited lithium sources and the safety problems caused by lithium dendrites restrict the progress and development of LIBs.[7–11] Therefore, alternative battery systems with low cost, abundant metal resources, and good safety performance should be urgently discovered.

In recent years, scientists have explored various metals, such as sodium, potassium, zinc, aluminum, and magnesium, for metal-ion batteries to replace lithium from various applications.[12–26] Among different metal-ion batteries, rechargeable magnesium-ion batteries (MIBs) are expected to be a potential candidate for large-scale energy storage systems owing to the following excellent intrinsic advantages. 1) Magnesium has a lower electrode potential (–2.37 V versus SHE) than Zn and Al metals. 2) Magnesium is a light metal with a density of 1.74 g cm^{-3} and is abundantly present in the earth's crust (i.e., approximately 2.1%, which is 10^4 times that of lithium metal). 3) Two electrons can be provided during redox reactions, leading to a higher theoretical volumetric capacity of 3866 mAh cm^{-3} than that of lithium metal (2046 mAh cm^{-3}). 4) A magnesium anode with higher stability than a lithium anode is significantly less susceptible to dendrite formation. Similar to other metal-ion batteries, the core components of MIBs are also anode, cathode and electrolyte. Commonly, the Mg^{2+} ions are released from the anode and inserted into the cathode during the discharge process, and the process is reversed during the charging process. However, the electrochemical performance of magnesium is different from that of lithium. The passivation layer formed between magnesium and ordinary electrolyte prevents the diffusion of Mg^{2+} ions and limits its reversible deposition from salt-containing aprotic electrolytes such as magnesium perchlorate, magnesium tetrafluoroborate, imide, carbonate, and nitrile. Hence, achieving reversible deposition/dissolution of Mg ions in the electrolyte is very important for MIBs.

Because Mg is active in an aqueous solution and easily forms a passivation layer on the surface, researchers have explored different organic systems to realize electrodeposition.[27–29] The concept of rechargeable MIBs was first raised in 1990. Gregory et al. constructed Mg//1.0 M *N*-ethylaniline magnesium chloride, 0.20 M $AlCl_3$, THF//Cu batteries, which demonstrated compatibility between Mg organoboranes electrolytes $(Mg(BPh_2Bu_2)_2$ or $Mg(BPhBu_3)_2)$ and Mg anodes.[30] Then, in 2000, Aurbach's group reported the first study on electrochemically deposited Mg metal.[31] Subsequently, the same research group prepared a high-voltage (>3 V) all-phenyl complex electrolyte as the product of the reaction between PhMgCl

M. Guo, C. Yuan, X. Yu
Department of Materials Science
Fudan University
Shanghai 200433, China
E-mail: yuxuebin@fudan.edu.cn
T. Zhang
College of Materials Science and Technology
Nanjing University of Aeronautics and Astronautics
Nanjing 210016, China
E-mail: zhangtengfei@nuaa.edu.cn
The ORCID identification number(s) for the author(s) of this article can be found under https://doi.org/10.1002/smll.202106981.

DOI: 10.1002/smll.202106981

and $AlCl_3$ in THF. Thereafter, Mg-ion liquid electrolytes such as HMDSMgCl-$AlCl_3$/THF, $MgAl_2$-$AlCl_3$/DMC, and $Mg(TFSI)_2$-DME, have been rapidly developed.[32–34] However, some difficult challenges are yet to be solved. The low oxidation decomposition potential and compatibility with the cathode material of the Grignard reagent system limit its application. More electronegative elements, such as N, O, or Cl, substitute Grignard carbanion, which can form a more stable complex anion combined with the strong Lewis acid in the system.[35–37] This complex anion has better oxidation resistance and enhances the anode stability in the electrolyte. At the same time, excessive Cl^- ions can be adsorbed on the surface of the magnesium anode, destroy the formation of the passivation layer, and enhance the electrodeposition of Mg^{2+} ions.[38,39] The combination of Cl^- ions and Mg^{2+} ions to form $MgCl^+$ ions can reduce the migration barrier, thereby increasing the migration rate. However, the formation of $MgCl^+$ also causes a decrease in energy density and difficulty in cathode intercalation. Moreover, when the potential exceeds 2.5V, Cl^- ions would corrode the battery components and thus affecting the electrochemical window and cycle life of the battery.[40–43] Nevertheless, some recent studies have confirmed that dendrite growth occurs during the process of magnesium-ion deposition, particularly at low operating temperatures, localization of anode edge overpotential and high charging rates.[44] Furthermore, conventional organic solvents contained in common liquid electrolytes are flammable and volatile.

Solid-state electrolytes have attracted significant interest for use in electrochemical energy storage technologies because they do not have the problems of passivation, dendrite growth, and corrosion of Mg anode.[45–47] Owing to their good safety performance, solid-state electrolytes can circumvent the problems of volatile and explosive organic solvents. In this review, solid-state magnesium electrolytes are systematically summarized from oxides, hydrides, chalcogenides, metal-organic frameworks (MOFs), and polymers. Furthermore, the migration mechanism of Mg^{2+} ions is comprehensively combed according to the different types. The review covers a broad and deep interdisciplinary discussion, including that on materials science, chemistry, surface engineering, and polymer science. The perspective in designing solid-state electrolytes will motivate industries to develop different applications of MIBs. Therefore, studies on solid-state electrolytes are important to address the fundamental challenges of electrochemical properties, and for the practical applications of next-generation MIBs in diverse areas.

2. Solid-State Electrolyte

Similar to the development route of all-solid-state lithium battery electrolytes, all-solid-state magnesium battery electrolytes are classified into five categories: oxides, hydrides, chalcogenides, metal–organic frameworks (MOFs) and polymers. **Figure 1** summarizes the advantages, disadvantages, and development routes of the five main types of solid-state magnesium electrolytes in recent years. In this section, the structure, ionic conduction mechanism, and improvement strategy of these five classifications will be systematically discussed.

2.1. Oxides

The ceramic based oxides with the general formula of $A_xM_y(XO_4)_3$ were first used as solid-state electrolytes for MIBs. The oxide $A_xM_y(XO_4)_3$ have two similar crystal structures: β-$Fe_2(SO_4)_3$-type (monoclinic symmetry, $P21/n$ space group) and natrium-super-ionic-conductor(NASICON)-type (rhombohedral symmetry, $R\bar{3}c$ space group) structures. Both of them are three-dimensional (3D) network structures based on a covalent skeleton $[M_2(XO_4)_3]$, which consists of MO_6 octahedron and XO_4 polyhedron sharing all angles. The size of these channels (4.5–4.7 Å) is larger than the edges of magnesium tetrahedra (3.3–3.7 Å). As shown in **Figure 2**a, the NASICON-type structure is more symmetrical than $Fe_2(SO_4)_3$-type structure and has a sufficiently large gap to form a suitable channel for Mg^{2+} ion transport. The well-ordered and stable $Zr_2P_3O_{12}$ (lantern) units allow smooth ion migration, resulting in high ionic conductivity, particularly at high temperatures.[48] In 1987, Ikeda et al. first reported the Mg-Zr-PO_4 system, which was applied in solid-state magnesium electrolytes.[49] When the stoichiometric composition of the system was $Mg_{0.5}Zr_2(PO_4)_3$ (MZP), the material exhibited the highest ionic conductivities of 2.9×10^{-5} and 6.1×10^{-3} S cm^{-1} at 400 and 800 °C, respectively. X-ray diffraction (XRD) measurement revealed the $R\bar{3}c$ structure of MZP, which is same to that of $NaZr_2(PO_4)_3$.

Further efforts have been made to understand magnesium ionic conductivity mechanisms and enhance the conductivity at low temperatures of the oxide solid electrolyte. First, researchers found that different synthesis processes and sintering temperatures influence the phase structure and compactness of the material.[50] Compared to the solid-state method, the sol-gel method allows precursors to mix more uniformly during the preparation process. Thus the sol-gel method reduces the sintering temperature and avoids the generation of impurities phase.[51] Unlike MZP containing second-phase $Zr_2O(PO_4)_2$ prepared by the solid-state method, the single-phase MZP was synthesized by Kazakos-Kijowski et al. using the sol-gel method at 900 °C.[49,51] Anuar and Adamu's groups prepared monoclinic single-phase MZP by a sol-gel method. They found that with the increase in sintering temperature, the density of the material (Figure 2c) and the grain size decreases, thus effectively reducing the grain boundary resistance in Mg^{2+} ion transport.[52,53] Figure 2b shows that upon sintering MZP above 850 °C, monoclinic MZP decomposed to its orthorhombic phase, $Zr_2O(PO_4)_2$. After high-temperature sintering and long-term annealing at 900 °C, the second phase is transformed into MZP (Figure 2d). At a sintering temperature of 1300 °C, the maximum relative density reaches 99% of the theoretical density resulting in low values of the grain boundary resistance. Liang et al. synthesized $Mg_{0.5}Ce_{0.2}Zr_{1.8}(PO_4)_3$ electrolyte nanopowders using the liquid-feed flame spray pyrolysis method and obtained a conductivity of 3×10^{-6} S cm^{-1} at 280 °C by increasing the density of the material and reducing the thickness of the electrolyte.[54] The variation in the Mg^{2+} ion conductivity as a function of temperature for various oxides is shown in Figure 2e.

In addition to optimizing the preparation method, anion and cation substitution can also improve the Mg^{2+} ion conductivity of MZP. The influence of the substitution of Zr^{4+}

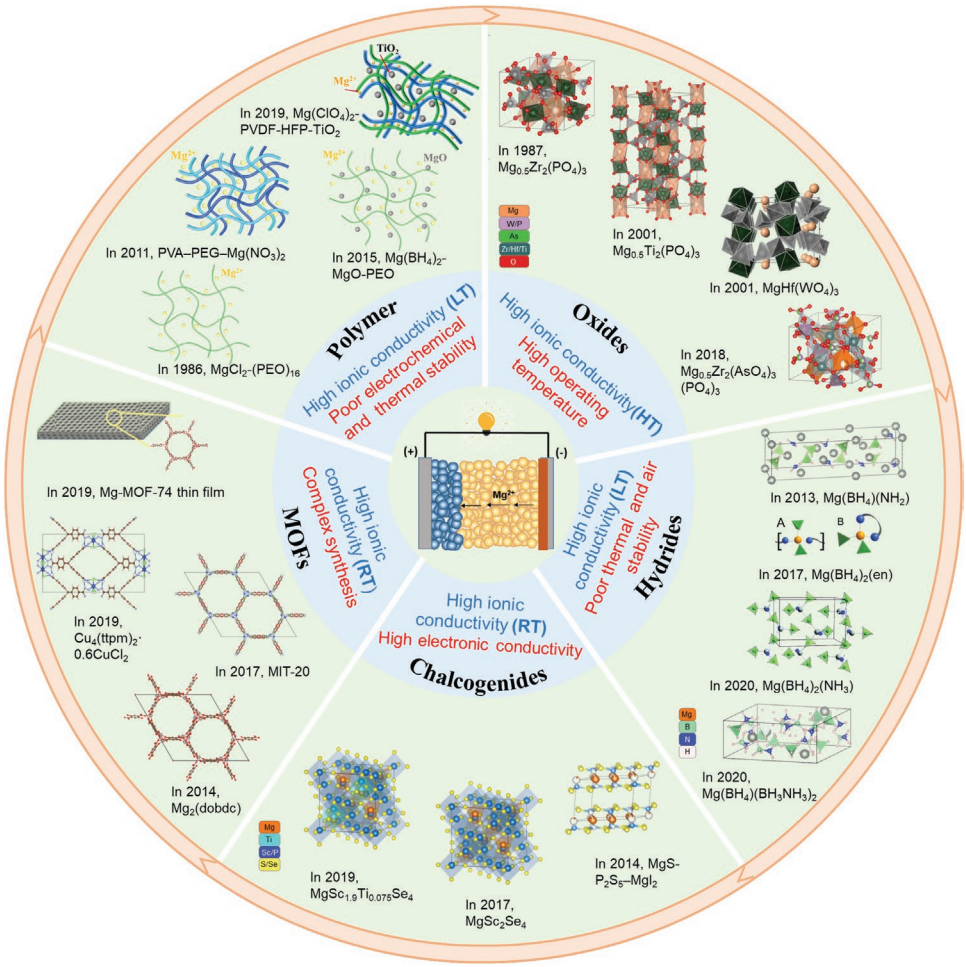

Figure 1. The various kinds and developments of solid-state electrolyte in MIBs.

ion with a smaller cation such as Fe^{3+}, Zn^{2+}, and Al^{3+} in the MZP structure has been studied by Anuar and co-workers.[55,56] The concentration of Mg^{2+} interstitial ions increased with the increase of the substitution element, leading to the enhancement of the conductivity and migration amount of Mg^{2+} ion in the compound. The substitution of Zr^{4+} ions with larger radii cations can improve the ion channels, reduce activation energy, and increase the conductivity.[57] For instance, the partial substitution of the tetravalent Zr^{4+} site in $MgZr_4P_6O_{24}$ by pentavalent Nb^{5+} significantly reduces the activation energy of the Mg^{2+} ion migration and enhances the conductivity.[58,59] On further development of a series of three-dimensionally well-ordered NASICON-type Mg^{2+} ion conductors, $(Mg_xHf_{1-x})_{4/(4-2x)}Nb(PO_4)_3$ ($0.05 \le x \le 0.3$) exhibited a higher conductivity (2.1×10^{-6} S cm^{-1}) than $Mg_{0.7}(Zr_{0.85}Nb_{0.15})_4(PO_4)_6$ (1.1×10^{-7} S cm^{-1}) at 400 °C due to the lower activation energy for the Mg^{2+} migration (63.9 kJ mol^{-1}) than that (92.0 kJ mol^{-1}) of β-$Fe_2(SO_4)_3$-type $Mg_{0.7}(Zr_{0.85}Nb_{0.15})_4(PO_4)_6$.[60,61]

A similar improvement strategy can also be applied to $Mg_{0.5}Ti_2(PO_4)_3$ (MTP) materials. Compared with Zr^{4+} (80 Å), the ionic radius of Ti^{4+} (68 Å) is much smaller; therefore, MTP has an isostructural lattice with the NASICON at room temperature. Barth et al. first prepared the MTP material by the sol-gel method.[62] Makino et al. synthesized a series of samples of $Mg_{0.5+y}(Me_yTi_{1-y})_2(PO_4)_3$ (Me = Cr, Fe) and found that the cell volume of $Mg_{0.5}Ti_2(PO_4)_3$ changed little with the Mg-ion insertion, which seems to be advantageous in terms of durability.[63,64] The insertion limit of the Mg^{2+} ion is determined by the mobility rather than the number of available sites for the Mg^{2+} ion. Takahashi et al. prepared TM-doped (TM = Fe, Mn, Co, and Nb) MTP and evaluated its crystal structure and electrical conductivity (**Figure 3**a,b).[65] It was found that the doping of Fe, Mn, and Co caused lattice contraction in the *c*-axis direction, which may strengthen the Mg–O_2 bond and shorten the Mg–O_2 distance, thereby increasing the conductivity of Mg^{2+}. In contrast, the Nb-doped sample exhibited the smallest conductivity (1.1×10^{-4} S cm^{-1} at 600 °C) and the maximum activation energy (102 kJ mol^{-1}), which may be due to the decrease in the Mg interstitial concentration and the increase in the Mg–Mg distance. Takahashi et al. further investigated Al-doped MTP and predicted the suitable lattice size for Mg ion transport.[66] For trivalent-doped titanium phosphates, the optimum lattice volume was estimated to be 1.304 nm^3 for the Mg-ion conduction. Halim et al. prepared $Mg_{0.5+x/2}Si_{2-x}Al_x(PO_4)_3$ with the NASICON-type structure by replacing Zr^{4+} (0.72 Å) with Si^{4+} (0.41 Å) to construct a suitable tunnel size for the Mg^{2+} ion

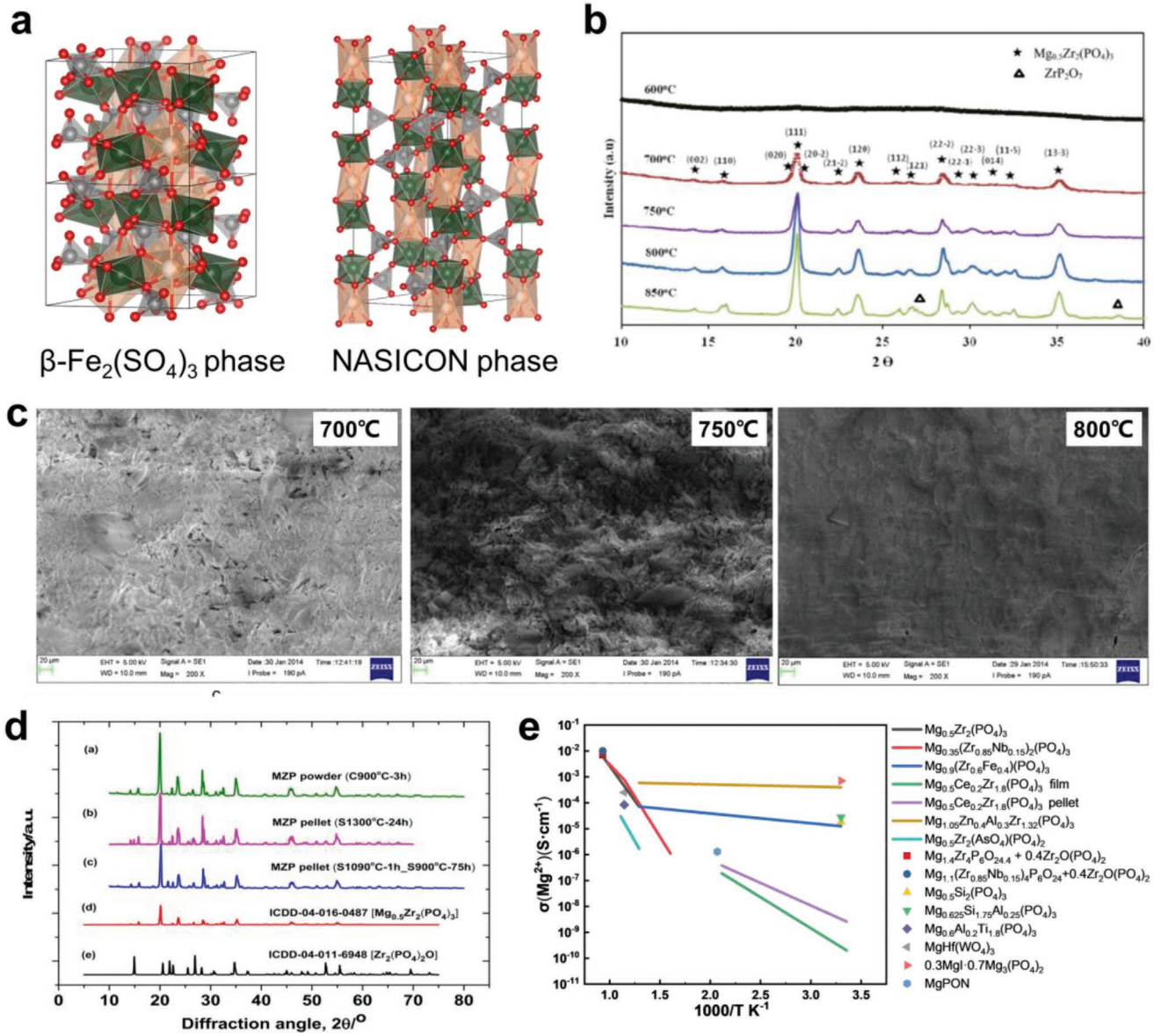

Figure 2. a) The crystal structure of β-$Fe_2(SO_4)_3$ and NASICON phase. b) XRD patterns of $Mg_{0.5}Zr_2(PO_4)_3$ sample sintered at different temperatures. Reproduced with permission.[52] Copyright 2014, Elsevier c) The cross-sectional SEM micrographs of $Mg_{0.5}Zr_2(PO_4)_3$ pellets sintered at different temperatures. Reproduced with permission.[52] Copyright 2014, Elsevier. d) XRD patterns for $Mg_{0.5}Zr_2(PO_4)_3$ powder calcined at 900 °C for 3 h and $Mg_{0.5}Zr_2(PO_4)_3$ pellet sintered at 1300 °C for 24 h; $Mg_{0.5}Zr_2(PO_4)_3$ pellet sintered at 1090 °C for 1 h, cooled down to 900 °C, and then annealed for 75 h. Reproduced with permission.[53] Copyright 2016, American Chemical Society. e) Temperature dependence of the Mg^{2+} ionic conductivity of different oxides

migration, thereby improving the conductivity.[67] Further, an improved ionic conductivity of 2.78×10^{-5} S cm^{-1} was achieved at room temperature through Al^{3+} doping.[68] Nomura et al. synthesized $Mg_{1.15}Zr_4(P_{0.95}Si_{0.05}O_4)_6$ by the sol–gel method to partially replace the phosphate skeleton with Si^{4+}.[69] This improved the compactness of the sintered specimens and the conductivity are both improved (1.4×10^{-5} S cm^{-1} at 530 °C).

Additionally, researchers found that the conductivity can be improved by introducing a second phase.[59,70,71] A $Mg_{1+x}Zr_4P_6O_{24+x}$+$xZr_2O(PO_4)_2$ composite was synthesized by intentionally changing the starting material mixing ratio to the nonstoichiometric ratio.[72] The microscopic dispersion of the second phase of $Zr_2O(PO_4)_2$ in the compound significantly increases its relative density. However, the $Zr_2O(PO_4)_2$ phase exhibits an insulation property, and its excessive addition will lead to a decrease in the conductivity. The $Mg_{1.4}Zr_4P_6O_{24.4}$+$0.4Zr_2O(PO_4)_2$ composite has the highest conductivity (6.92×10^{-3} S cm^{-1} at 800 °C); however, it has high activation energy is still high (1.14 eV). Therefore, further improvements can be made by replacing Zr^{4+} with Nb^{5+} to prepare $Mg_{1.1}(Zr_{0.85}Nb_{0.15})_4P_6O_{24.4}$+$0.4Zr_2O(PO_4)_2$, which increases the conductivity to 10^{-2} S cm^{-1} at 800 °C.[59]

In addition to the above-mentioned phosphate-based oxide solid electrolytes, some other kinds of oxide electrolytes have also been investigated. Ahmad et al. prepared a magnesium-based solid electrolyte MgI_2–$Mg_3(PO_4)_2$ composite via ball

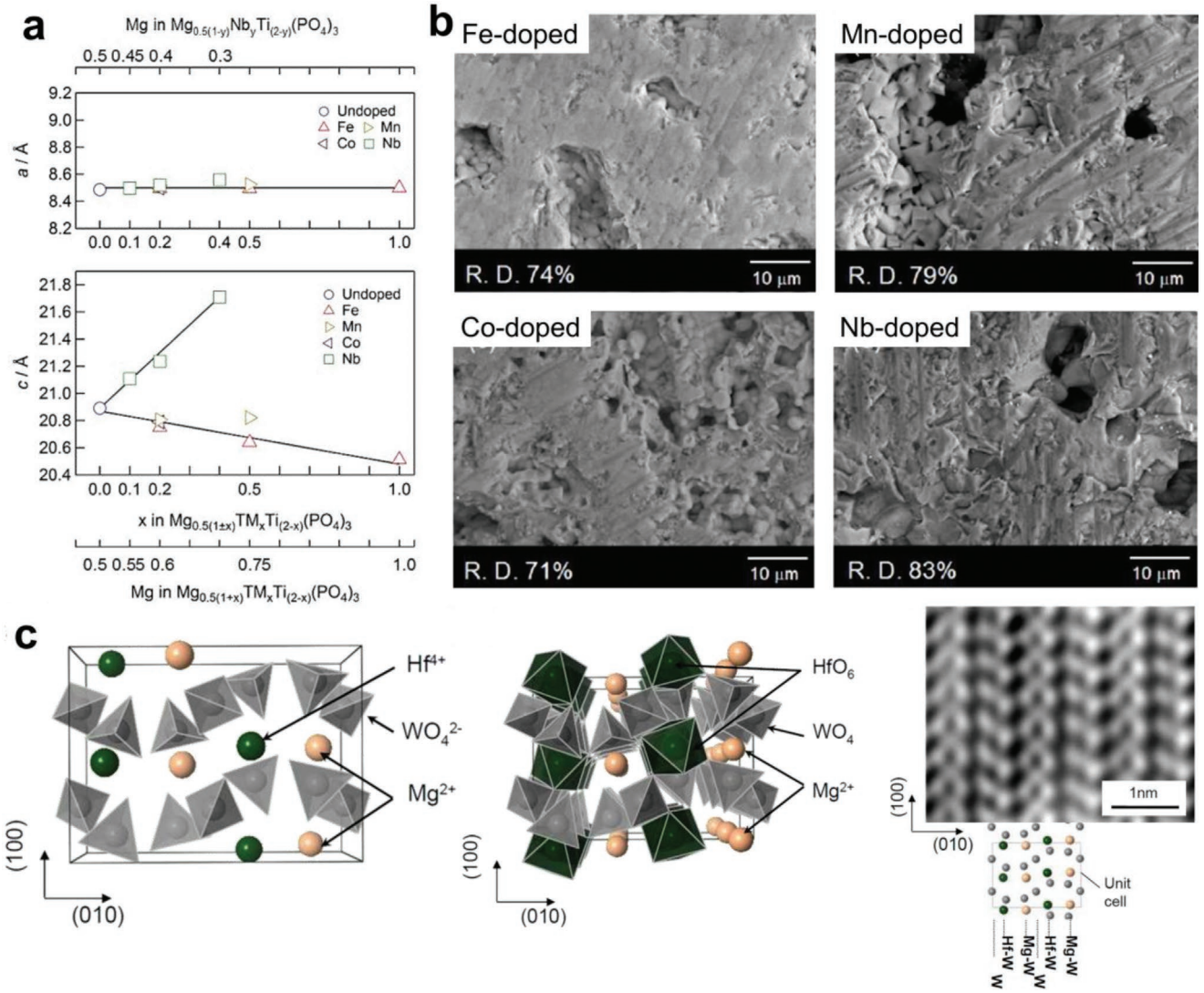

Figure 3. a) Lattice constant of Fe, Mn, Co and Nb-doped $Mg_{0.5}Ti_2(PO_4)_3$ as a function of the concentration of TM or Mg. Reproduced with permission.[65] Copyright 2012, Trans Tech Publications Ltd. b) SEM images of Fe-, Mn-, Co-doped $Mg_{0.5}Ti_2(PO_4)_3$ sintered at 1150 °C for 2 h and Nb-doped $Mg_{0.5}Ti_2(PO_4)_3$ at 1200 °C for 10 h. R. D. means the relative density of the samples calculated from the theoretical value. Reproduced with permission.[65] Copyright 2012, Trans Tech Publications Ltd. c) The most energetically stable structure of $MgHf(WO_4)_3$, in which Mg^{2+} and Hf^{4+} arrange one after another in the (010) direction, calculated by VASP and HAADF-STEM image in $MgHf(WO_4)_3$, viewed from the (001) cross-section. Reproduced with permission.[74] Copyright 2011, American Chemical Society.

milling.[73] The binary 30% MgI_2-70% $Mg_3(PO_4)_2$ has a maximum conductivity of 7.0×10^{-4} S cm^{-1} at room temperature, ≈2080 times higher than that in pure $Mg_3(PO_4)_2$. Sulaiman et al. synthesized $Mg(NO_3)_2$-$x$$Al_2O_3$ and $Mg(NO_3)_2$-xMgO composites by sol–gel method, which exhibited high Mg^{2+} conductivities of 4×10^{-4} S cm^{-1} and 10^{-6} S cm^{-1} at room temperature, respectively.[70,71] Omote et al. developed a novel ion conductor comprising magnesium hafnium tungstate ($MgHf(WO_4)_3$), which showed a high conductivity of 1.4×10^{-5} S cm^{-1} at 600 °C.[74] The reason for the improved conductivity is presumably attributed to the weakening of the Mg–O bonding strength, leading to an increase in the Mg^{2+} ion conduction space (Figure 3c). Su et al. reported plasma-assisted atomic layer deposition growth and characterization of $Mg_{2.4}P_2O_{5.4}$ thin films as a solid-state electrolyte.[75] The film exhibited an ionic conductivity of 1.6×10^{-7} S c m^{-1} at 500 °C, with an activation energy of 1.37 eV.

Despite the efforts made by many scholars in this field, oxide materials still have some problems in the field of magnesium solid electrolytes. Most synthesis techniques and applications need to be performed at significantly high temperatures, whereas the conductivity is too low at moderate temperature for practical utilization. Therefore, it is necessary to further ameliorate the preparation process to improve the conductivity and attempt to develop other types of materials, that can work at low temperatures.

2.2. Hydrides

Magnesium borohydride, $Mg(BH_4)_2$, has a high hydrogen capacity (14.9 wt%) with a small enthalpy change of Mg (41 kJ mol^{-1} H_2, theoretically estimated), which has received

wide attention as one of the potential candidates for advanced hydrogen storage materials.[76–80] In the meantime, many scholars have investigated $Mg(BH_4)_2$ as a magnesium ionic electrolyte.[31,81–84] In 1957, Connor et al. first realized the electrodeposition of magnesium from ether solutions of $Mg(BH_4)_2$.[82] However, the deposited material was not pure magnesium, and contained 9.4 wt% boron. In 2012, Mohtadi et al. proved that the electrochemical performance when $Mg(BH_4)_2$ as the electrolyte of the MIBs in glyme is better than that of THF, and they were the first to achieve reversible deposition/exfoliation in a halogen-free inorganic salt.[84] The interaction between Mg^{2+} and BH_4^- is weak, leading to an easy dissociation in DME. Despite the fact that DME has a slightly lower dielectric constant (7.2) compared to THF (7.4), its chelating performance could enhance this dissociation. Moreover, adding $LiBH_4$ to a Mg $(BH_4)_2$ electrolyte can significantly improve the current density of Mg deposition with a coulombic efficiency of 94%, and result in pure magnesium deposition. Shao et al. also developed an electrolyte based on $Mg(BH_4)_2$, diglyme and optimized concentration of $LiBH_4$ and obtained 100% coulombic efficiency. They believed that from the kinetics viewpoint, the $LiBH_4$ additive as the second coordination ligand $(BH_4)^-$ can increase the concentration and speed up the stripping process at the electrode surface, which accounts for the enhanced coulombic efficiency.

The above studies demonstrated the possibility of $Mg(BH_4)_2$ application in liquid electrolytes. On the other hand, the Mg^{2+} ions are coordinated with the BH_4^- group through a strong coulombic interaction and confined in tetrahedral cages composed of BH_4^-, thereby resulting in a low Mg^{2+} conductivity at room temperature (10^{-12} S cm^{-1}) in a solid-state electrolyte.[85,86] Therefore, reducing the binding between the anions and Mg^{2+} ion can accelerate ion migration in the solid-state through partial substitution of BH_4^- with larger ions or neutral molecules, such as AlH_4^-, NH_3BH_3, or NH_2^-.[87–91] Matsuo et al. using first-principles molecular dynamics (FPMD) simulations, proposed that the replacement of BH_4^- with AlH_4^- can enhance the Mg^{2+} ion conduction.[87] Through theoretical simulation, Ikeshoji et al. further found that the Mg ions were capable of moving outside the cage after introducing larger-sized AlH_4^- anions by substitution of 20% BH_4^-.[86] In 2013, Noritake et al. synthesized $Mg(BH_4)(NH_2)$ as a potential solid-state electrolyte by ball milling $Mg(BH_4)_2$ and $Mg(NH_2)_2$ under argon for 2h and heating at approximately180 °C.[92,93] Later in 2014, Higashi et al. described the structure of $Mg(BH_4)(NH_2)$, as shown in **Figure 4**a, and predicted using density functional theory (DFT) calculation that it is a band gap insulator with an ionic bonding characteristic.[94] Figure 4f shows the reversible Mg deposition and stripping behavior by cyclic voltammograms. The Mg^{2+} ionic conductivity of 10^{-6} S cm^{-1} was obtained at 150°C for $Mg(BH_4)(NH_2)$, which is three orders of magnitude higher than that of $Mg(BH_4)_2$.[95] Then, Ruyet et al. studied the influence of ball milling and heat treatment on the Mg^{2+} conductivity in $Mg(BH_4)(NH_2)$.[96] The pure Mg^{2+} ionic conductivity can be as high as 3×10^{-6} S cm^{-1} at 100 °C, which is three orders of magnitude higher than that reported by Higashi. This can be attributed to the formation of a glass-ceramic-like composite material with the presence of an additional amorphous phase.[94] The same group further synthesized the crystalline single-phase compound-$Mg_3(BH_4)_4(NH_2)_2$ with a high thermal stability, resulting in a high Mg^{2+} ionic conductivity of 4.1×10^{-5} S cm^{-1} at 190 °C and low activation energy (0.84 eV) at 100 °C.[97] Figure 4e shows the Arrhenius plots of ionic conductivity as an inverse function of temperature for various hydrides.

Recently, Roedern et al. prepared $Mg(en)(BH_4)_2$ by ball milling ethylenediamine (en, $NH_2(CH_2)_2NH_2$) and $Mg(BH_4)_2$.[98] The introduction of a chelated en ligand can significantly improve the Mg^{2+} ionic conductivity from $<10^{-12}$ S cm^{-1} to 5×10^{-8} at 30 °C. It is crucial to reduce the number of en ligands that coordinate with the Mg^{2+} cation from three in $Mg(en)_3(BH_4)_2$ to one in $Mg(en)(BH_4)_2$, to obtain an asymmetric mixing of Mg^{2+} with one en and two BH_4^- (Figure 4b). The symmetry of the anions and the binding effect on the Mg ions decreases, which is more conducive to the Mg^{2+} ionic conduction. The anodic current during the reverse sweeps between –0.2 and 0.5 V is shown in Figure 4g, strongly indicating the occurrence of the Mg conduction.

More recently, in 2020, Yan et al. synthesized $Mg(BH_4)_2 \cdot nNH_3$ (n = 1, 2, 3, and 6) and found that with the decreasing n, the conductivity of Mg^{2+} ion increases.[89] The crystal structure of $Mg(BH_4)_2 \cdot NH_3$ is shown in Figure 4c. Based on this, Yan et al. further explored the influence of non-stoichiometry of NH_3 doping on the Mg^{2+} ionic conductivity.[90] $Mg(BH_4)_2 \cdot 1.6NH_3$ with stable amorphous structure was synthesized by ball milling and combined with 75 wt% MgO nanoparticles.[90] The Mg^{2+} ionic conductivities of the nanocomposite are ≈10^{-5} S cm^{-1} at room temperature and ≈10^{-3} S cm^{-1} at 70 °C. Furthermore, Figure 4h shows that the composite exhibits good cyclic stability and reversibility of Mg plating/stripping for more than 15 cycles. Although oxide is not conductive, the presence of an insulator will produce a defective, highly conductive layer along the interface between the conductive and insulating phases.[99,100] Simultaneously, the addition of MgO can stabilize the amorphous phase of the $Mg(BH_4)_2 \cdot 1.6NH_3$ during the cycle and improve ionic conductivity.

In the $Mg(BH_4)_2 \cdot 2(NH_3BH_3)$ system, Mg^{2+} is tetrahedrally coordinated to two borohydrides (BH_4^-) and two ammonia boranes (NH_3BH_3) by ball milling $Mg(BH_4)_2$ and NH_3BH_3 (Figure 4d).[88] A $Mg/Mg(BH_4)_2 \cdot 2(NH_3BH_3)/Mo$ solid-state battery was assembled, which achieved a conductivity of 1.3×10^{-5} S cm^{-1} at 30 °C.

In recent years, some researchers have analyzed the structure and ion transport mechanism of $Mg(BH_4)_2$ through calculations and structural characterization. Burankova et al. investigated the dynamics of $Mg(BH_4)_2$-$diglyme_{0.5}$ on the atomic level by means of quasielastic neutron scattering supported by DFT calculations and infrared radiation (IR) and nuclear magnetic resonance (NMR) spectroscopy.[101] The results revealed that a high Mg^{2+} conductivity can be achieved through the chelating ability of diglyme but can negatively impact the thermal stability of the electrolyte. Heere et al. used synchrotron radiation powder X-ray diffraction (SR-PXD), quasi-elastic neutron scattering (QENS), and synchrotron X-ray total scattering experiments with the corresponding pair distribution function (PDF) analysis to analyze the structure of $Mg(BH_4)_2$ before and after ball milling.[102] The corresponding PDFs showed that the structure of $Mg(BH_4)_2$ in the amorphous state still maintains a short-range order, which is the same as the crystalline state,

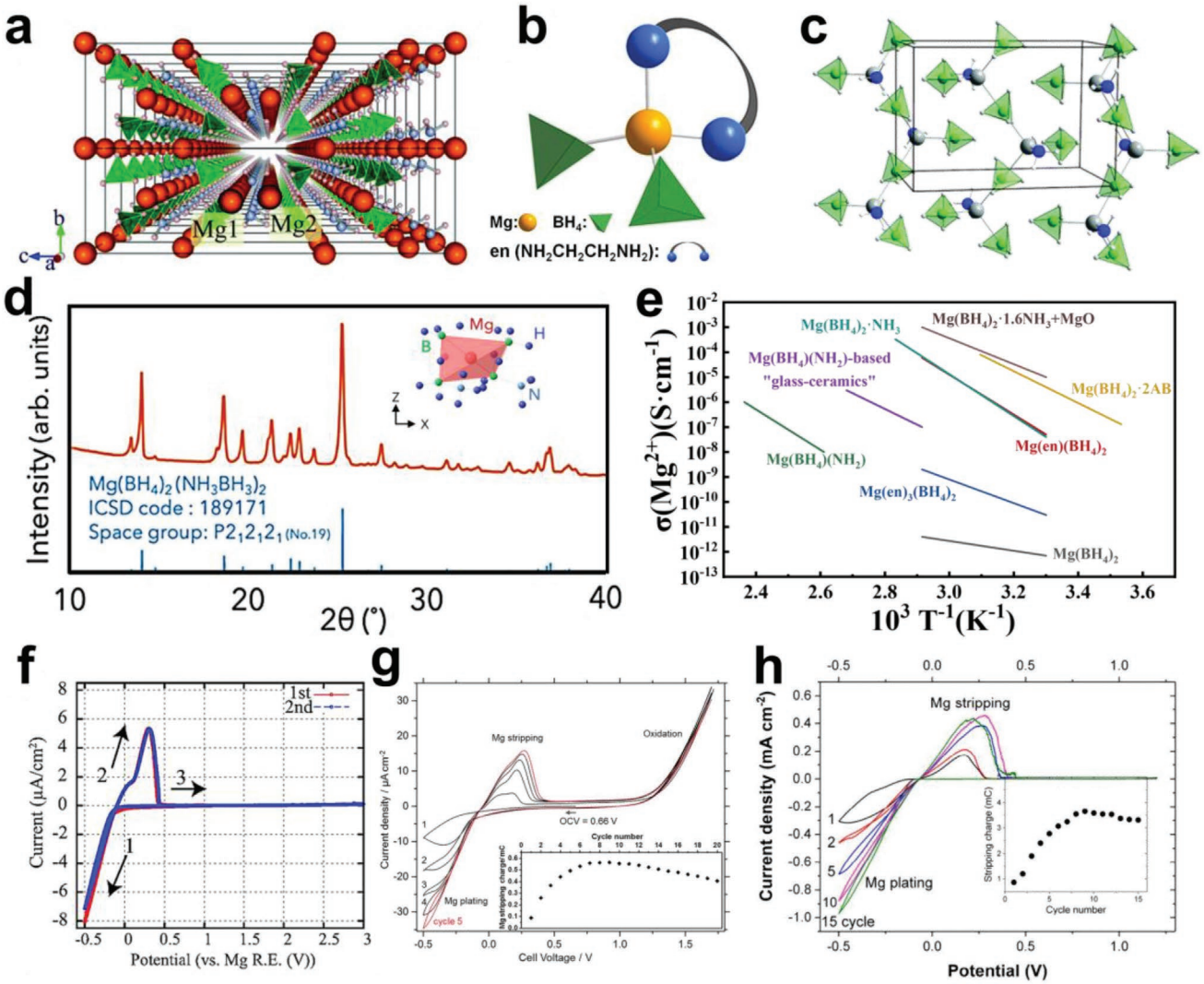

Figure 4. a) The crystal structure of $Mg(BH_4)(NH_2)$. Reproduced with permission.[94] Copyright 2014, Royal Society of Chemistry. b) The tetrahedral arrangement of coordinating ions in $Mg(en)_1(BH_4)_2$. Reproduced with permission.[98] Copyright 2017, Nature Publishing Group. c) The crystal structure of $Mg(BH_4)_2{\cdot}NH_3$. Reproduced with permission.[89] Copyright 2020, Royal Society of Chemistry. d) XRD patterns of $Mg(BH_4)_2{\cdot}2(NH_3BH_3)$, the insert shows the crystal structure $Mg(BH_4)_2{\cdot}2(NH_3BH_3)$. Reproduced with permission.[88] Copyright 2020, American Chemical Society. e) Arrhenius plots of ionic conductivity as a function of the inverse of temperature for various hydrides. f) Cyclic voltammograms of $Pt/Mg(BH_4)(NH_2)/Mg$. Reproduced with permission.[94] Copyright 2014, Royal Society of Chemistry. g) Cyclic voltammograms of $Pt/Mg(en)_1(BH_4)_2$ /Mg cell at 60°C. Reproduced with permission.[98] Copyright 2017, Nature Publishing Group. h) Cyclic voltammograms of Au/Mg $(BH_4)_2{\cdot}1.6NH_3$@MgO/Mg cell. Reproduced with permission.[90] Copyright 2020, American Chemical Society.

and the one-dimensional ion-transport channel in the amorphous $Mg(BH_4)_2$ still exists. The QENS data showed a higher fraction of activated rotations in the amorphous sample, which is helpful to improve the Mg^{2+} conductivity.

2.3. Chalcogenides

Similar to the Li^+ oxide-based electrolytes, the synthesis process of the Mg^{2+} oxide-based electrolytes require long sintering times and cumbersome steps. However, the products always exhibit poor mechanical properties with large interface impedance. By substitution of sulfur ions for oxygen ions, lower-temperature synthesized Mg^{2+} solid-state electrolytes (SSEs) present a weaker bonding strength between the sulfur and magnesium ions. Their lower electronegativity and larger radius provide a wider migration tunnel for ions and typically exhibit much more flexibility. In this case, Mg sulfide-based materials have been paid much attention due to their promising high ionic conductivity. Inspired by the Li_2S-P_2S_5-LiI system, Shigematu and co-workers prepared amorphous sulfide electrolytes of $MgPS_3$-MgI_2 by mechanical milling.[103] The sulfide glasses in the $60MgPS_3$-$40MgI_2$ system exhibited an Mg^{2+} ionic conductivity of 3.1×10^{-7} S cm^{-1} at 200 °C. Meanwhile, MgS-P_2S_5 is also expected as one of the potential Mg^{2+} solid-state electrolytes. The glass ceramics of MgS-P_2S_5-MgI_2 were prepared by

Tatsumisago and co-workers using a mechanochemical technique and subsequent heat treatment, which exhibited an Mg^{2+} ionic conductivity of 2.1×10^{-7} S cm^{-1} at 200 °C.[104]

Nevertheless, the ionic conductivity of these sulfide-based Mg^{2+} electrolytes is still far less than that in analogous Li^+/Na^+ electrolytes. For instance, Tatsumisago et al. measured Na_3PS_4 with a high conductivity of up to 10^{-4} S cm^{-1} at room temperature, which can be further improved by Si doping.[105,106] In 2016, Kanno and co-workers reported $Li_{9.54}Si_{1.74}P_{1.44}S_{11.7}Cl_{0.3}$ with an exceptionally high conductivity of 25×10^{-3} S cm^{-1} at room temperature.[107] Later, the cubic structure of Na_3SbS_4 and Na_3PSe_4 were found to exhibit high ionic conductivities owing to the well-constructed diffusion channels Consequently, structural frameworks with high Mg mobility should decrease the migration energy barriers with the increasing volume per anion, in the following order $O^{2-} < S^{2-} < Se^{2-} < Te^{2-}$.[107,108] Thus, Ceder et al. reported a representative work on maximizing the volume per anion of the structure and designing a series of Mg-ion conductors with the stoichiometry MgX_2Z_4 (where Z = S and Se and X = In, Y, and Sc) (**Figure 5**a).[109] In these spinel structures, a vacant octahedral site between two tetrahedral sites provides a pathway for the migration of Mg^{2+}. The Rietveld refinement results of the synchrotron XRD pattern for $MgSc_2Se_4$ in Figure 5b shows that the structure is in a pure $MgAl_2O_4$-type spinel (*Fd-3m*) phase. In the high-purity $MgSc_2Se_4$ phase, the fast Mg^{2+} mobility (10^{-4} S cm^{-1} at room temperature) with a low migration barrier (≈370 ± 90 meV) has been confirmed by both Mg NMR relaxometry and electrochemical impedance spectroscopy, which agrees with the conductivity extrapolated from the ab initio molecular dynamics simulation (Figure 5c,d). However, 0.04% of the total conductivity was attributed to the electronic conductivity, which is higher than that of the current solid-state electrolytes (10^{-4}–10^{-6} S cm^{-1} at room temperature).

According to Ceder et al.'s investigation, a chalcogenide-rich phase should have a lower electronic conductivity, which is dependent on the content of the Se element. More recently, Guo and co-workers synthesized different amounts of Se-rich (5 wt% and 10 wt%) phases of $MgSc_2Se_4$ to decrease the electronic conductivity.[110] For a sample with 5 wt% Se in excess, the electronic conductivity decreased to 2.1×10^{-8} S cm^{-1} while the ionic conductivity was 7.2×10^{-5} S cm^{-1}, which is the same as that observed in the sample without Se-excess. Instead, the electronic conductivity increased significantly to 1.1×10^{-5} S cm^{-1} while the ionic conductivity was lowered to 2.7×10^{-5} S cm^{-1}. This indicates that excessive Se has a negative impact on decreasing the electronic conductivity, which is also accompanied by side reactions. Thus far, the proposed strategies to lower the electronic conductivity by the implementation of Se-rich phases and aliovalent doping (Ti^{4+} and Ce^{4+}) have led to ineffective neutralization of the electronic conductivity.

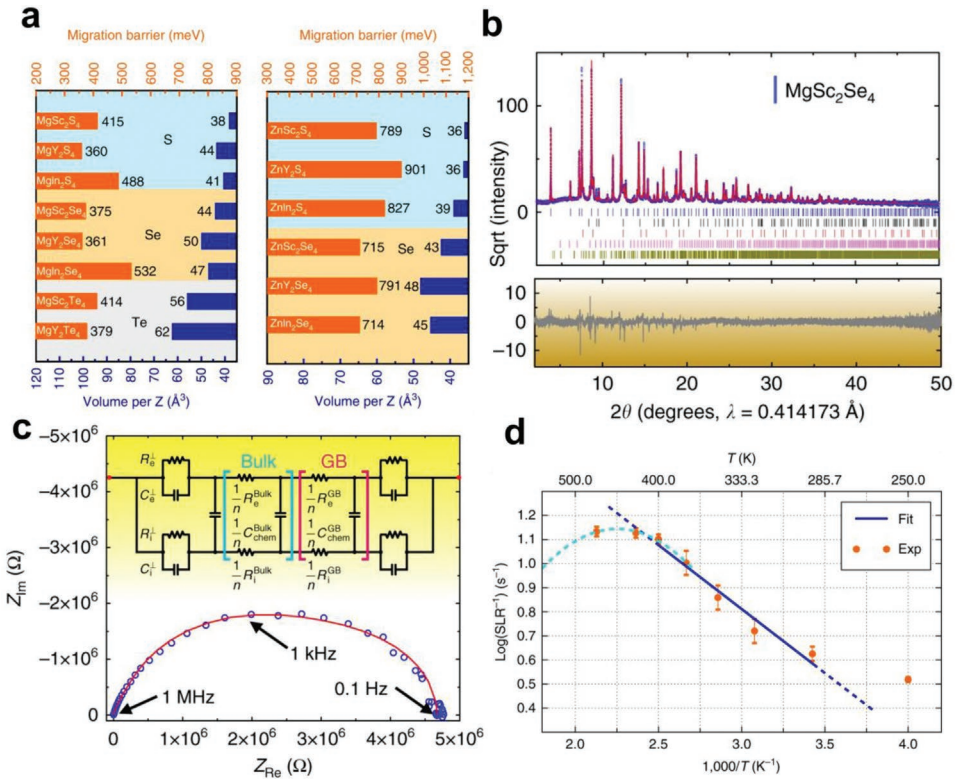

Figure 5. a) Computed Mg and Zn migration barriers (orange bars in meV) in AX_2Z_4 spinel and volume per anion (blue bars) using first-principles calculations, respectively, with X = Sc, Y, and In, and Z = S, Se, and Te. b) Rietveld refinement of the synchrotron XRD pattern for $MgSc_2Se_4$. Reflections corresponding to $MgSc_2Se_4$ (blue), Mg (black), MgSe (red), Sc_2O_3 (magenta), and Sc_2Se_3 (dark yellow) are shown with tick marks of the respective colors. c) Impedance spectrum of the Ta/$MgSc_2Se_4$/Ta cell, and the circuit utilized in the fitting of the impedance data. d) spin-lattice relaxation data of ^{25}Mg recorded as a function of temperature; the blue line indicates the Arrhenius fit. Reproduced with permission.[109] Copyright 2017, Nature Publishing Group.

However, owing to both the fast ionic and electronic conduction properties, spinel $MgSc_2Se_4$ can reversibly insert/extract the Mg^{2+} ions as cathode materials.

2.4. MOFs

Metal–organic frameworks (MOFs), or porous coordination polymers, are compounds that are assembled by metal ions/cluster and organic ligands and extend infinitely in one, two, or three dimensions.[111,112] They have attracted considerable attention owing to their large specific surface area and exceptional tunability on pore dimension without affecting the underlying topology. Furthermore, because of mild synthesis conditions and ease of functionalities, they are widely investigated in the fields of adsorptive separation, catalysis, drug delivery, energy storage and many others.[112,113] Moreover, their single-ion conductivity makes them promising candidates for application in the SSEs, especially for the transport of multivalent ions, such as Mg^{2+} and Al^{3+}.[114] Considering the diversity of the MOF structures and the progress of nanotechnology, MOFs with internal mobile ions can be assembled with desired pore structures, which has great potential for internal cation migration. The MOFs with open metal cation sites can incorporate lithium isopropoxide into their structures to produce a solid-state electrolyte with fast ionic conductivity.[115] However, unlike lithium-ion conductive MOFs, the investigations that focus on magnesium ionic conductivity are just emerging in the research of magnesium-ion SSEs, but many milestone results have been achieved.

To achieve the expected ion migration, the corresponding target metal ions should be first introduced within the MOF host. A relatively convenient strategy is to immerse the MOFs in a salt solution. followed by the filtration and drying processes.[116,117] A representative work by Long et al. reported the uptake of lithium isopropoxide into the MOF with the open metal cation sites, leading to a high lithium ionic conductivity of 3.1×10^{-4} S cm^{-1} at 300 K.[117] Soon afterwards, inspired by this concept, Long and co-workers prepared and characterized a series of Mg^{2+} solid-state electrolytes using a similar approach.[118] Considering that Mg^{2+} ion has a smaller radius and higher charge density than Li^+ ion, it is easier to achieve rapid migration of the Mg^{2+} ions using the MOFs solid electrolytes with suitable pore sizes and a high density of open metal sites capable of coordinating nucleophilic anions. Then, Mg_2(dobdc) and its expanded analog Mg_2(dobpdc) (dobpdc = 4,4″-dioxidobiphenyl-3,3″-dicarboxylate) with sufficient pore size and rich open metal sites were chosen as the hosts for Mg^{2+} (**Figure 6**a). Figure 6b shows the three symmetrical anion coordination sites of Mg_2(dobpdc). The impregnation of a magnesium halide salt within the MOFs produced a series of composite materials. The conductivity increased with the decreasing anion basicity of the guest electrolyte salts. The resulting values of the activation energies shown in Figure 6d were determined by fitting the variable-temperature conductivity data according to the Nernst–Einstein relation from 0.11 to 0.19 eV. By increasing the pore size, the larger organic linker decreases the polarity of the MOF surface, while there is no change in the one-dimensional Mg^{2+} chains. Consequently, the ionic conductivity of Mg was significantly increased to over four orders of magnitude, approaching as high as 0.25 mS cm^{-1}.[118]

On the other hand, the synthesized MOFs were modified to form anionic frameworks with charge-balancing mobile cations, which often requires cumbersome procedures and conditions. The size of the pore apertures in the MOFs is much larger than that of metallic cations, which provides the transport pathway and determines the transference numbers.[119] The aliovalent ion doping and substitution have led to the mobile Mg^{2+}. In 2017, Dinca et al. reported a novel Cu(II)-azolate metal-organic framework (MOF) with tubular pores, which experiences a crystal transition between neutral and anionic species by reaction with halide or pseudohalide salts.[115] The formation of a single-ion solid-state electrolytes depends on the binding and settlement of the halide/pseudohalide anions, while the cations move freely within one-dimensional pores. The free cations are not only limited to monovalent ions (such as Li^+, Na^+), divalent ions such as Mg^{2+}, can also be substituted within Cu-azolate MOF. The Li^+-, Na^+-, and Mg^{2+}- loaded materials exhibit high ionic conductivity values of 4.4×10^{-5}, 1.8×10^{-5}, and 8.8×10^{-7} S cm^{-1}, respectively (Figure 6e). Later, the same group introduced a Cu-azolate material, $Cu_4(ttpm)_2$ (H_4ttpm = tetrakis(4-tetrazolylphenyl)methane) as a host MOF owing to its multiple binding sites for trapping anions.[120] This abundance in the anionic binding sites in $Cu_4(ttpm)_2$ leads to a high density of independent cations, which significantly accelerates the cationic conductivity, particularly for the Mg^{2+} ion.[121] As shown in Figure 6c, two equivalent halides can be installed per Cu_4(tetrazole)$_8$ secondary building units through soaking the MOF in a solution of MX_n (M = Li^+, Mg^{2+}, X = Cl^-, Br^-). Appropriate open metal sites in the host promote the stoichiometric rebinding of the fixed anions. This process provides the potential to increase the density of the highly mobile cations and maximize the cation transference numbers by altering the character of the immobilized anion. The bromide salts lead to higher Mg^{2+} ionic conductivity than the chlorides within the $Cu_4(ttpm)_2 \cdot 0.6CuCl_2$ as a solid-state electrolyte. Remarkably, an ionic conductivity of 1.3×10^{-4} S cm^{-1} was measured in MOF-$MgBr_2$ as shown in Figure 6f, which presented a promising concept for further investigating the application of the MOFs as the SSEs for multivalent ions such as Mg^{2+}. Although these rising MOFs are potential alternatives to the current polymer/ceramic electrolytes, the study of MOF-based electrolytes at a nascent stage. In addition to proper ionic conductivity, their chemical/electrochemical stability, mechanical strength, and process ability need to be evaluated before they can be declared suitable as solid-state electrolytes for commercial application.[122]

2.5. Polymers and Composites

Polymers have gradually received increasing attention in the field of solid-state electrolytes because of their good flexibility, light weight, and easy processing.[123,124] The solid polymer electrolyte (SPE) is generally formed by a polymer matrix such as polyethylene oxide (PEO), polyvinyl alcohol (PVA), polyethylene carbonate (PEC), polyvinyl pyrrolidone (PVP), and polyacrylonitrile (PAN) and a magnesium salt (e.g., $MgCl_2$, $Mg(ClO_4)_2$, $Mg(NO_3)_2$, Mg(TFSI)$_2$ and Mg(Tf)$_2$).[123] As shown in

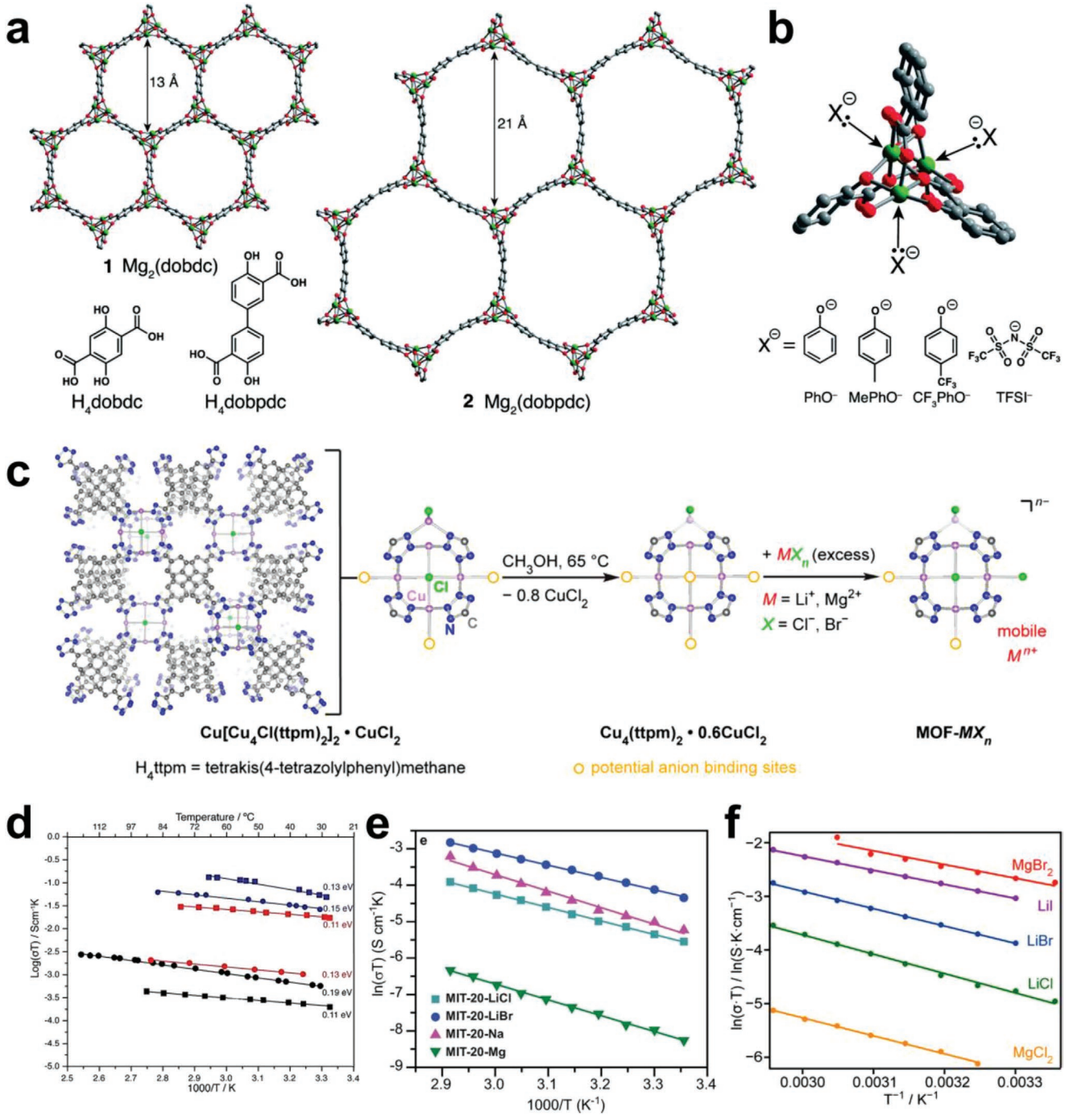

Figure 6. a) Structures of the metal-organic frameworks Mg_2(dobdc) and Mg_2(dobpdc), as viewed along the c-axis. Reproduced with permission.[118] Copyright 2014, Royal Society of Chemistry. b) The open coordination sites at the vertices of the pore that interact with nucleophilic guest species. Reproduced with permission.[118] Copyright 2014, Royal Society of Chemistry. c) Synthesis procedure of $Cu[(Cu_4Cl)(ttpm)_2]_2{\cdot}CuCl_2$, $Cu_4(ttpm)_2{\cdot}0.6CuCl_2$, and the Target MOF-$MX_n$. Temperature-dependent conductivity plots for the respective MOF-MX_n electrolytes. Reproduced with permission.[121] Copyright 2019, American Chemical Society. d) Ionic conductivities as a function of temperature for Mg_2(dobdc)-*X* and Mg_2(dobpdc)-*X* (Mg_2(dobdc) is depicted as circles and Mg_2(dobpdc) as squares, the *X* $Mg(OPhCF_3)_2$ is shown in black, $Mg(TFSI)_2$ in red, both magnesium salts in blue). Reproduced with permission.[118] Copyright 2014, Royal Society of Chemistry. e) Ionic conductivities as a function of temperature for MIT-20-*X* (*X* = LiCl, LiBr, Na, Mg) in the range of 25 to 70 °C. Reproduced with permission.[115] Copyright 2017, American Chemical Society. f) Ionic conductivities as a function of temperature for MOF-MX_n electrolytes. Reproduced with permission.[121] Copyright 2019, American Chemical Society.

Figure 7a, the magnesium salt is complexed with the polymer to form a continuous cross-linking network. On the one hand, the ionic conductivity of the SPE depends on the dissociation ability of the salt in the polymer matrix, which provides the

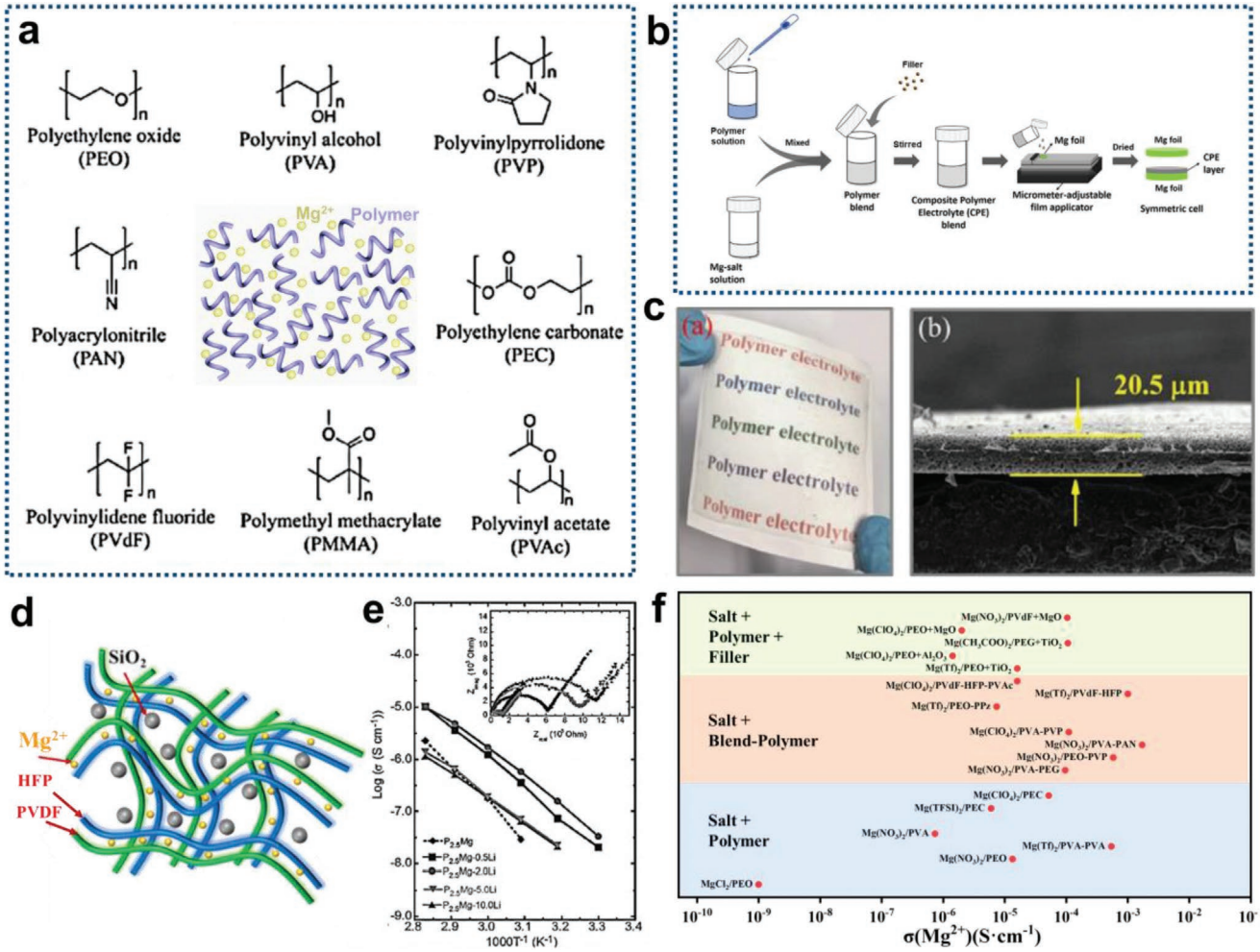

Figure 7. a) Scheme of polymer electrolytes for MIB and molecular structures of polymer hosts. Reproduced with permission.[123] Copyright 2020, IOP Publishing Limited. b) Procedure to synthesize the composite polymer electrolyte. Reproduced with permission.[146] Copyright 2019, American Chemical Society. c) Optical image of a large-scale flexible solid polymer electrolyte and cross-section SEM image to characterize the thickness of solid polymer electrolyte. Reproduced with permission.[136] Copyright 2020, Elsevier. d) Structural diagram of $Mg(TFSI)_2$-PE. Reproduced with permission.[148] Copyright 2020, American Chemical Society. e) Temperature dependence of the ionic conductivity for P2.5Mg with differing LiFSI concentrations 0.5Li, 2.0Li, 5.0Li, 10.0Li (inset: Nyquist plots at 80 °C). Reproduced with permission.[153] Copyright 2019, Nature Publishing Group. f) Temperature-conductivity plots of the various CPEs.

Mg^{2+} ions for ionic conduction. On the other hand, ion transport associated with the segmental motion of the polymer also affects the ionic conductivity. Therefore, significant conductivity of the SPE is only observed above the glass transition temperature of the system. Below the glass transition temperature, the magnesium ion chain conduction of the polymer electrolyte is hindered by the crystalline region, resulting in a lower ionic conductivity. Therefore, the ionic conductivity of the SPE material at room temperature can be improved by lowering the glass transition temperature and increasing the flexibility of the structure.

Most polymer electrolytes reported PEO as the common polymer host due to its high solubility and low vitrification temperature. In 1986, Yang and co-workers reported the first SPE magnesium-ion conductor composed of PEO complexing with the magnesium salt ($MgCl_2$).[125,126] Thereafter, researchers also tried to synthesize the complexes of PEO with other magnesium salts such as $Mg(TFSI)_2$, $Mg(NO_3)_2$, and $Mg(Tf)_2$, for which the ionic conductivities at room temperature were 10^{-7}, 1.34×10^{-5}, 3.21×10^{-8} (50 °C) S cm^{-1}, respectively.[127–130] Although the conductivity is relatively high, the direct current (DC) results showed that the main conductive ions in these electrolytes are anions, and due to the strong electrostatic interaction between the Mg ion and ether chain oxygens, the Mg-ion movement is hindered.[131,132] Further research results showed that with the increase in the Mg salt concentration in the system, the Mg^{2+} ion concentration in the system increases along with an increase in its conductivity. Combining the XRD, atomic force microscopy (AFM) and Fourier-transform infrared spectroscopy (FT-IR) results indicated that the increase in the conductivity is related to the decoupled Mg^{2+} ions with large aggregates in the SPEs.[133,134] A simple SPE system was reported by Ramesh et al. based on [P(VdF-HFP)] and $Mg(Tf)_2$.[135,136] The Mg^{2+} ionic conductivity reached a maximum of $\approx 10^{-3}$ S cm^{-1} at ambient

temperature when 40 wt% of the $Mg(Tf)_2$ salt was incorporated. The presence of cathodic and anodic current peaks indicated that Mg^{2+} ion conduction in PEC. However, further increasing the salt concentration will increase the crystalline region in the material and hinder the transmission of the magnesium ions.

To further improve the conductivity, researchers have attempted to blend different polymers to form a polymer matrix. The blending of polymers is an effective way to develop new polymeric materials with improved mechanical stability. The two main advantages of the blending system are simplicity of preparation and controllability of physical properties by compositional regulation.[137,138] Polu et al. developed a PVA-PEG-$Mg(NO_3)_2$ system by a simple solvent casting technique, and the conductivity of the system was measured to be 9.63×10^{-5} S cm^{-1} at room temperature.[139] The Mg^{2+} conductivities of $Mg(ClO_4)_2$ in the PEO-PVP-$Mg(NO_3)_2$ and PVA-PAN-$Mg(NO_3)_2$ systems are 5.8×10^{-4} and 1.7×10^{-3} S cm^{-1} at room temperature, respectively.[140–142] Researchers also explored the ionic conductivity of $Mg(ClO_4)_2$ in different double-hybrid polymer matrices, such as PVC-PAN, PVA-PVP, PVdF-HFP-PVAc.[137,142,143] Among them, PVA-PAN-$Mg(ClO_4)_2$ has the highest conductivity of 2.96×10^{-4} S cm^{-1} at room temperature and PVdF-HFP-PVAc-$Mg(ClO_4)_2$ has the highest electrochemical stability of 4 V.[142,143] Ma and co-workers constructed a solid-state Mg hybrid ion full battery using an SPE of a PVDF-HFP film filled with PEO/ILMSE, which can cycle for over 5000 times with 90% capacity retention. As shown in Figure 7c, the battery with an ultra-thin electrolyte layer has good flexibility and outstanding sewability, which provides the possibility for the development of wearable energy storage devices in the future.

In addition, passive/active nanofillers (e.g., TiO_2, Al_2O_3, SiO_2, MgO nanoparticles) can also affect the conductivity of the material.[144–150] Such systems are referred to as nano-composite polymer electrolytes (NCPEs). The NCPEs are generally composed of two phases, one is an SPE as the host matrix, and the other is an inert filler material as the dispersoid (Figure 7d). Figure 7b shows the specific preparation process of the NCPEs. The size of the dispersed particles and the chemical properties/dielectric constant of the nanofillers play an important role in improving the different physical properties of the composite electrolyte system. Dissanayake and co-workers prepared $PEO_9Mg(ClO_4)_2$ by incorporating 10 wt% nano-porous Al_2O_3 filler grains by the solvent casting technique.[147] The increased conductivity of these micron and nanocomposite polymer electrolytes is thought to be caused by the Lewis acid–base interactions between the O-Oh surface groups on the filler surface and the migrating ionic material. These interactions produce additional jumping sites and favorable ion motion pathways.[151] The active nanofiller MgO can increase the migration number of the Mg^{2+} ions and improve the ionic conductivity because it can ionize the Mg^{2+} ions.[144] Shao et al. developed a nanocomposite polymer electrolyte consisting of PEO, $Mg(BH_4)_2$, and MgO nanoparticles.[149] Longer-chain glymes showed a strong coordination ability with the Mg^{2+} ion through their increased electron donor and chelating ability, thus enhancing the dissociation of the salt $Mg(BH_4)_2$ in PEO. This results in a high coulombic efficiency of 98% for Mg plating/stripping, high cycling stability, and highly efficient Mg intercalation/de-intercalation in Mo_6S_8.

Inspired by the liquid electrolyte, Aziz and co-workers attempted to add LiFSI to the PEC-$Mg(TFSI)_2$ SPE to increase the conductivity of the material (Figure 7e).[152,153] The results proved that the addition of the LiFSI salt can promote the ionization of $Mg(TFSI)_2$ without affecting its oxidation stability. Cui et al. further discovered that the addition of the Li salt can generate an SEI (solid electrolyte interphase) layer capable of transporting the Mg ions on the surface of the electrode, such that the electrolyte can continue the electrochemical cycle stably for a long time.[154]

3. Mechanism

Currently, unlike the significant development of lithium-ion solid-state electrolytes, research activities focusing on the progress of all-solid-state magnesium batteries are comparatively slow. Only a few studies have demonstrated the long-term cycling of all-solid-state magnesium batteries, while several companies have begun to verify the concept of all-solid-state lithium-ion batteries for mass production. Owing to the high charge density of magnesium ions, the transport and diffusion of magnesium ions inside the solid-state electrolyte and the electrode interface are slow. Therefore, research on magnesium-ion solid-state electrolytes is mainly focused on improving the conductivity of magnesium ions. To better understand the ion transport mechanism of electrolytes and provide the basic criteria for the design of novel electrolytes, further discussion of the magnesium-ion transport mechanism in different kinds of solid-state electrolytes should be understood in depth.

3.1. Inorganic Solid-State Electrolytes

3.1.1. Oxides

Zirconium phosphates as monovalent and divalent cation conducting compounds have been investigated since 1976. The framework of zirconium is characterized by its ability to host monovalent cations (e.g., Li^+, Na^+), which exhibit excellent ionic conduction behaviors. Divalent cations (e.g., Mg^{2+}) can migrate through the structures at high temperatures, which was verified through DC electrolysis experiments in the Tubandt setup. In the $Mg_{0.5}Zr_2(PO_4)_3$ structure, the magnesium cations generally occupy the mobile sites, with elongated antiprisms sharing triangular faces with the two adjacent ZrO_6 octahedra along the *c*-axis of the hexagonal cell. The anisotropic separation of these two ZrO_6 polyhedral in the c-direction determines the size of the bottleneck for the conduction pathway between two adjacent magnesium ions. An analysis of the refinement of the $Mg_{0.5}Zr_2(PO_4)_3$ phosphate crystal structure confirmed that the structure of the scandium tungstate type is stable below 1023 K.[155] A decreasing monoclinic angle β in the unit cell of the phosphate structure with the increasing temperature above 1023K, as well as the anisotropy of the thermal expansion, can lead to a phase transition to rhombohedral phase with a change in the unit cell symmetry. This is similar to the increase in the conductivities of complex hydrides due to the phase transition with the increasing temperature. This conclusion has also

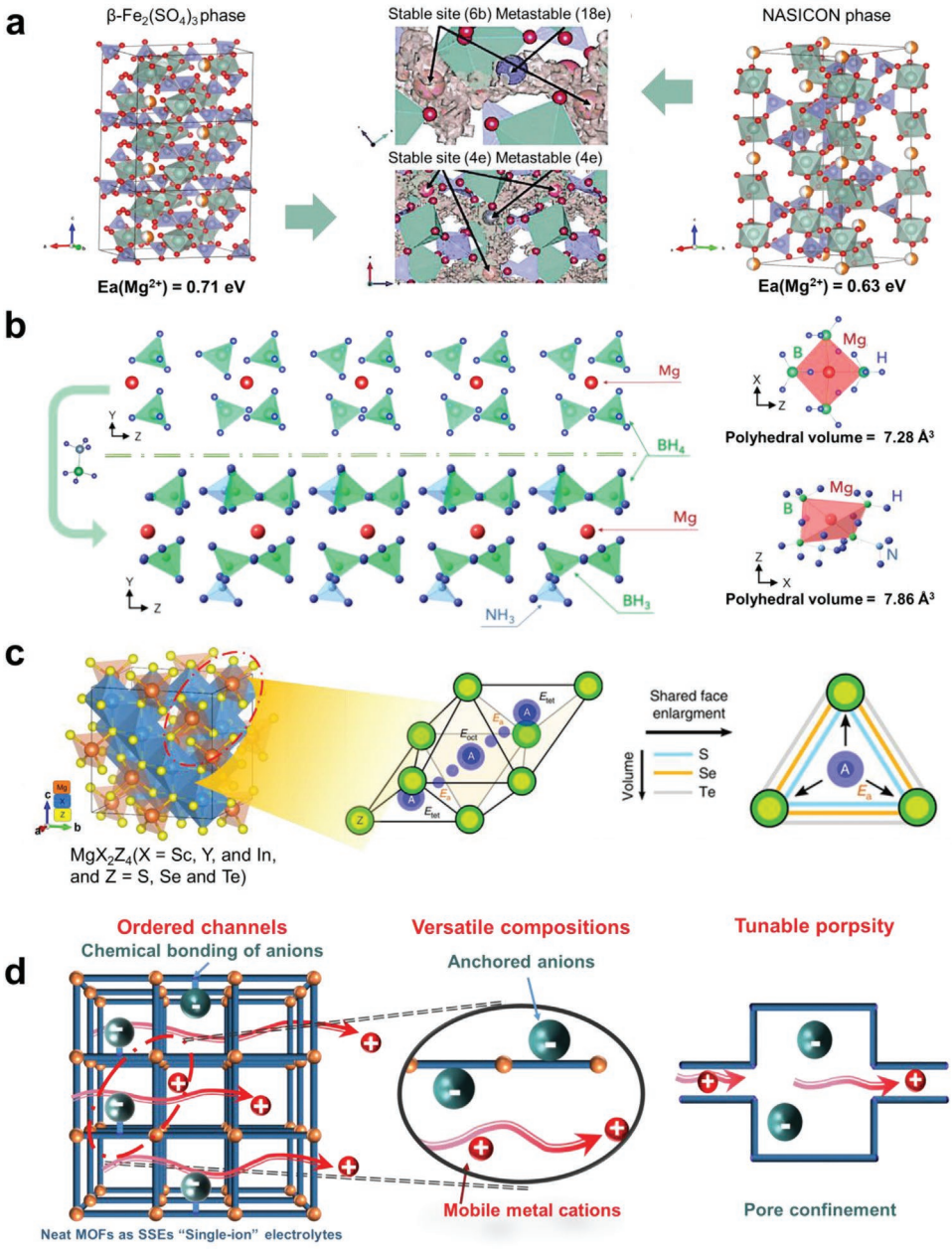

Figure 8. a) The migration of Mg^{2+} in $Mg_{0.5}Zr_2(PO_4)_2$. Reproduced with permission.[155] Copyright 2019, Royal Society of Chemistry. b) The migration of Mg^{2+} in $Mg(BH_4)_2$ and $Mg(BH_4)_2{\cdot}2(NH_3BH_3)$. Reproduced with permission.[88] Copyright 2016, American Chemical Society. c) The migration of Mg^{2+} in MgX_2Y_4. Reproduced with permission.[109] Copyright 2017, Nature Publishing Group d) The migration of Mg^{2+} in MOFs. Reproduced with permission.[114] Copyright 2020, Royal Society of Chemistry.

been supported via the phase transition of the zirconium phosphate framework by NMR. **Figure 8**a shows the trace of the Mg atom in the FPMD simulation at 1973 K. The results indicate that the migration energy of the Mg ions in the β-iron sulfate-type structure is less than that in the NASICON-type structure, which further explains the high conductivity of the NASICON-type structure of MZP.

As for the impact of element substitution on performance, the substitution of ions with different radii and valences can not only change the concentration of Mg^{2+} ion vacancies, but also change the structure of Mg^{2+} ion channels, thereby affecting the Mg^{2+} ionic conductivity of the material.[58,64,67] The unit cell parameters of the material are reduced after low-valence and small atomic radius cations doping, while the monoclinic $P21/n$ structure is still maintained. However, when the doping cation is a large cation such as Hf or Nb, the symmetry of the structure changes and the ion channel becomes larger. Some researchers have also verified that the addition of Fe, Mn, and Co in the MTP structures can strengthen the Mg–O bond and decrease the Mg–O distance, leading to an increase in the ionic

conductivity. Furthermore, introducing a second phase, such as $Zr_2O(PO_4)_2$, improves the ionic conductivity. The substitution of higher-valent cations Nb^{5+} for Zr^{4+} to form a solid solution can produce a Mg^{2+} cation vacancy in the grain. The combination with the second-phase $Zr_2O(PO_4)_2$ promotes microscopic dispersion and improves the conductivity behavior of Mg^{2+} ions at the grain boundary.

3.1.2. Hydrides

Owing to Mg^{2+} ions in $Mg(BH_4)_2$ located in the tetrahedral cages surrounded by four BH_4^- ions and the migration of Mg^{2+} ions limited by the strong coulombic interactions with BH_4^- ions, the conductivity of magnesium ions in $Mg(BH_4)_2$ is very low at room temperature. After the partial substitution of the BH_4^- ions with larger ions or neutral molecules, the volume of the anion tetrahedron increases, resulting in larger tetrahedral cages and easier migration of the magnesium ions in the structure.[88,89,93] The distance between the nearest Mg atoms in $Mg(BH_4)(NH_2)$ is 3.59 Å, less than that in the $Mg(BH_4)_2$, indicating that this structure may be conducive to the jump diffusion of Mg^{2+}.[95] Furthermore, the network of di-hydrogen N-Hδ+$\cdots\delta$H-B bonds surrounding Mg^{2+} has a high degree of structural flexibility, thus promoting the movement of Mg^{2+} ions and resulting in increased ionic conductivity.[93]

A highly flexible structure can form in the $Mg(BH_4)_2$-NH_3 system owing to the neutral molecule exchange within the lattice, leading to fast moving interstitial Mg^{2+} ions. A di-hydrogen bond can be easily formed between a partially negatively charged hydrogen in borohydrides (BH_4^-), acting as an acceptor group, and a partially positively charged hydrogen in a neutral NH_3 molecule. This di-hydrogen bond binds the BH_4^- ions, which weakens the limits on the interstitial Mg^{2+} ions. DFT verified the above results, and the calculation results also suggested that the migration energy barrier of $Mg(BH_4)_2$ is much larger than that of $Mg(BH_4)_2 \cdot NH_3$.[89,90] In particular, the $Mg(BH_4)_2$-(NH_3BH_3) system processes the highest conductivity at room temperature.[88] The increase in the Mg^{2+} ionic conductivity is owing to the Mg-B bond distance in $Mg(BH_4)_2 \cdot 2(NH_3BH_3)$. The volume of the tetrahedron around Mg became larger than $Mg(BH_4)_2$, which weakened the binding effect on the Mg^{2+} ion.[79,156] Furthermore, the distance between the NH_3BH_3 molecule and the Mg^{2+} ion is large, which can make Mg^{2+} shift or rotate flexibly, thus improving the conductivity. Figure 8b shows a schematic diagram of the ion channels of $Mg(BH_4)_2$ and $Mg(BH)_2 \cdot 2(NH_3BH_3)$ with the calculated size of the ion channels, respectively, which further verifies the above conclusion.

3.1.3. Chalcogenides

A statistical analysis from the Inorganic Crystal Structural Database suggested that the Mg^{2+} ions prefer an octahedral coordination environment instead of a tetrahedral one. Consequently, structural frameworks with high Mg mobility should properly tailor the Mg residing in its unfavorable tetrahedral coordination environment. Spinel structures are therefore expected to be logical Mg^{2+} conductors since the electrostatics of the cation arrangement ensures a stable tetrahedral site for Mg^{2+}. In the spinel structures, the ion migration between two tetrahedral sites (tet) occurs via a vacant octahedral site (oct), which face-shares with the tetrahedral sites, following the migration topology tet-oct-tet. According to the design criteria, a magnesium scandium selenide spinel, $MgSc_2Se_4$, was demonstrated to present faster magnesium ionic conductivity and is therefore a more attractive candidate among magnesium solid-state electrolytes.[109] The DFT calculations also indicate that lower migration barriers can be obtained by choosing larger anions (S < Se < Te), where the Mg^{2+} cations can diffuse through the large triangular faces (Figure 8c).

3.2. Organic Solid-State Electrolytes

the smaller size and greater charge density of the magnesium ions than that of lithium ions, the synthesis of solid-state electrolytes with suitable pore sizes can easily accommodate the bigger polar species, leading to a faster conduction of the magnesium ions than that in the oxides or hydrides electrolytes. The MOFs with a high density of open metal sites capable of coordinating nucleophilic anions can serve as the host framework for the magnesium ions.[115] As shown in Figure 8d, these open metal sites may accelerate the cation mobility, inhibiting the migration of the nucleophilic anions.[114] Furthermore, the uniformity of cation plating/stripping upon charging/discharging can be improved owing to the microporous feature and ordered channels. Moreover, MOFs with tunable porous structures (pore size, pore shape, and pore polarity) can act as ion sieves that preferentially promote cation transfer.[11] Even though the nucleophilic electrolyte, such as $Mg(TFSI)_2$ or $Mg(OPhCF_3)_2$, interacts strongly with a single crystallite, ion transportation between crystallites is not fast. However, the non-nucleophilic anion (e.g., TFSI or $OPhCF_3$) shows no preference for absorption in the framework. More importantly, a synergistic conductivity enhancement is demonstrated from these guest electrolytes owing to the different interactions within the framework and transport processes. Accordingly, frameworks with dual guest salts present fast ionic conductivities of approximately 0.1 mS cm^{-1} at room temperature.[118]

3.2.1. Solid Polymer Electrolytes

Solid polymer electrolytes have been paid significant attention owing to their high mechanical toughness, low cost, and compatibility with large-scale assembly compared to liquid electrolytes. However, the main challenge of polymer electrolytes is the effective improvement of ionic conductivity for practical applications. For monovalent cation salts, such as Li^+, Na^+, mobile ion species can be dissociated into monovalent ions in a polymer matrix. The lithium ions are located in the coordination sites of polymer segmented chains. The lithium ions could jump from one coordination site to another with the help of local segmental motions. In contrast, for Mg salts with monovalent anions, MgX_2, besides the fully dissociated ions, Mg^{2+} and X^-, mobile ion species of ionic complexes (e.g., MgX^+,

$Mg_2X_3^+$, MgX_3^-) also occupy a wide range of concentration in the polymer matrix. It means that a single ionic conductivity measurement cannot indicate the adequacy of the magnesium conduction, as the bulk conductivity may be dominated by anion migration.

In the SPEs above the glass transition temperature (T_g), the temperature dependence of the ionic conductivity is interpreted with the Vogel-Tamman-Fulcher (VTF) equation. Remarkably, the VTF behavior can be described as:

$$\sigma = \sigma_0 \exp[-B/(T - T_0)] \quad (1)$$

where σ is the ionic conductivity, σ_0 is the pre-exponential factor, B is the pseudo-activation energy, T is the temperature, and T_0 is the Vogel temperature (often $\approx T_g - 50$). At or above T_g (equilibrium glass transition temperature), the mobility of the polymeric segments is sufficiently active to provide ionic conduction. However, the migration of the ions below T_g exhibits almost no ionic conductivity, indicating that the ions are only shuttled along and between different complexing sites in the polymer matrix. The complicated nature of speciation of the ionic complexes has been illustrated through a myriad of techniques. For instance, the Mg^{2+} transference number was calculated to be 0.23 according to the Bruce–Vincent method, which is much smaller than that of univalent ions. Another case of the SPEs is the so-called polymer-in-salt with the increasing salt content, the polymer itself acts like the salt crystals binder to an extent that the ions transport at the interface between the salt particles and polymer matrix, thereby displaying a liquid-like behavior. The proposed conduction mechanism involves ion hopping between different salt clusters in a percolating manner, where the existence of a continuous network is necessary for the onset of the conductivity behavior.

4. Summary and Perspective

Since SONY commercialized lithium-ion batteries in the 1990s, the existing electrochemical system has gradually reached a bottleneck after more than 30 years of development and will gradually enter the "post-lithium-ion battery" era in the near future. The strong market demand will certainly promote the application of new materials, new systems, and new processes in the field of batteries to achieve great breakthroughs. Among the new electrochemical energy storage systems, rechargeable MIBs have continually received much attention owing to their advantages such as lower cost, more safety, and higher volumetric specific capacity than LIBs. However, unlike the widespread research and application of LIBs, the rechargeable MIBs face significant challenges on all fronts, including cathodes, anodes, and electrolytes. Particularly for electrolytes, a key component of the MIBs, limited research has not yet reached the evaluation stage to ensure the commercial feasibility of the technology. Previous research suggested that liquid electrolytes can easily react with magnesium anodes to form an SEI, which is unfavorable for ion transport. Instead, current efforts continue to develop new solid-state materials and understand their fundamental mechanism in depth.

Solid-state electrolytes are at the core of magnesium-ion solid-state batteries, which are promising candidates to achieve industrialization of MIBs from the laboratory. This review systematically summarizes the remarkable progress of different types of Mg-ion solid-state electrolyte over the past decades. Particularly in recent years, the magnesium ionic conductivity in various solid-state electrolytes has been increased to over 10^{-4} S cm^{-1} at room temperature, which is gradually narrowing the gap between the magnesium-ion solid-state electrolytes and traditional liquid electrolytes. **Table 1** shows the comparison of the advantages and disadvantages of various solid-state magnesium battery electrolytes. However, compared with the lithium-ion and sodium-ion, there are still relatively fewer reports on solid-state magnesium-ion conductors. In addition to ionic conductivity, other electrochemical properties of solid-state magnesium-ion conductors are often not comprehensively characterized, including ionic selectivity, electrochemical stability, chemical compatibility, mechanical property, and assembly technology. Consequently, very few rechargeable full cells have been implemented thus far.

Future research on magnesium-ion solid-state electrolytes can draw lessons from the mature strategy of lithium-ion/sodium-ion solid-state electrolytes. In particular, studying the electrode-electrolyte interface is helpful in improving the poor kinetics and thermodynamic stability. Herein, some future

Table 1. Advantages and disadvantages of various solid-state magnesium battery electrolytes.

Solid state electrolyte	Advantages	Disadvantages
Oxides	(1) High safety (2) High thermal stability (3) Facile manufacturing process (4) Good compatibility (5) easy integration with other SSEs	(1) Low flexibility (2) Rich grain boundaries (3) Relatively low cation transference number (4) High application temperature
Hydrides	(1) High safety (2) Light weight (3) Facile manufacturing process (4) Relatively high oxidation potential (5) Good interfacial/interparticle wetting ability	(1) High cost (2) Low flexibility (3) Limited thermal stability (4) Relatively low cation transference number
Chalcogenides	(1) Reasonable wetting ability (2) High mechanical strength (3) High conductivity at room temperature	(1) High cost (2) Low flexibility (3) High electronic conductivity
MOFs	(1) Reasonable wetting ability (2) High mechanical strength (3) "'Single-ion"' conduction (4) high cation transference numbers (5) High conductivity at room temperature	(1) Low flexibility (2) Tedious fabrication process (3) Rich grain boundaries (4) Safety issues from the residual solvents
Polymer	(1) High flexibility (2) Fine interfacial contact (3) Facile manufacturing process (4) Good compatibility and easy integration with other SSEs (5) High conductivity at room temperature	(1) Limited thermal stability (2) Week mechanical strength (3) Relatively low oxidation potential (4) Poor electrochemical

perspectives are presented based on magnesium solid-state electrolytes but are not limited to them. For instance, 1) In addition to improving the conductivity, the electrochemical window of solid-state electrolytes also needs to be optimized to ensure the reversible deposition and stripping of magnesium ions and reduce interfacial impedance. Currently, the electrochemical window of inorganic solid-state electrolytes has been reported to be up to 3 V, however, the corresponding conductivity is very poor. Therefore, artificial SEI and interfacial modification that can improve the electrochemical stability and maintain high ionic conductivity are potential research focus areas. 2) Mg–S batteries have attracted significant attention considering the safety characteristics, abundant reserves of both magnesium and sulfur and high volumetric energy density. Based on solid-state electrolytes, the Mg–S batteries can effectively solve the shuttle effect and prohibit dissolution of polysulfide, leading to improved capacity decay and cycling stability. 3) Moreover, investigating the migration mechanism of magnesium-ion in the fundamental redox reaction may further improve the electrochemical performance in a full cell. Utilizing more advanced characterization techniques and theoretical calculation approaches would significantly improve the mechanism of ion transportation, understanding of the performance of materials, and designing of battery systems. 4) The structure and composition design of composite solid-state electrolytes can be further optimized. To take full advantage of active fillers, it is necessary to form an interfacial ion conduction network between the polymer and the fillers. Therefore, a composite solid electrolyte with high inorganic filler content should exhibit higher conductivity, higher electrochemical stability, and higher cyclic stability. In contrast, composite inorganic electrolytes, such as a combination of chalcogenide and hydride, are designed to amplify the advantages of two or more inorganic materials, which are considered to achieve a breakthrough in solid-state electrolytes.

In summary, magnesium-ion solid-state electrolytes are currently still in a nascent stage. Substantial efforts have been made to improve the performance of batteries thus far, including modification of cathode and anode materials, and the synthesis of novel electrolyte systems. Fortunately, high energy-density systems that can outperform Li-ion batteries are attracting significant attention and practical and reliable Mg full cell might be soon realized.

Acknowledgements

This work was partially supported by the National Science Fund for Distinguished Young Scholars (51625102), the National Natural Science Foundation of China (51971065, 51802154, 52171180), the Innovation Program of Shanghai Municipal Education Commission (2019-01-07-00-07-E00028), the Fundamental Research Funds for the Central Universities (NS2020039), Open Fund of Key Laboratory of Materials Preparation and Protection for Harsh Environment (Nanjing University of Aeronautics and Astronautics), and Ministry of Industry and Information Technology (XCA20013-2).

Conflict of Interest

The authors declare no conflict of interest.

Keywords

rechargeable magnesium batteries, solid-state electrolytes, ion migration mechanisms, optimization strategies

Received: November 12, 2021
Revised: December 30, 2021
Published online: February 19, 2022

[1] J. M. Tarascon, M. Armand, *Nature* **2001**, *414*, 359.
[2] B. Dunn, H. Kamath, J. M. Tarascon, *Science* **2011**, *334*, 928.
[3] D. Larcher, J. M. Tarascon, *Nat. Chem.* **2015**, *7*, 19.
[4] A. Manthiram, X. Yu, S. Wang, *Nat. Rev. Mater.* **2017**, *2*, 16103.
[5] M. Guo, S. L. Zhong, T. Xu, Y. Q. Huang, G. L. Xia, T. F. Zhang, X. B. Yu, *J. Mater. Chem. A* **2021**, *9*, 23841.
[6] C. Wang, Z. Y. Guo, S. Zhang, G. D. Chen, S. M. Dong, G. L. Cui, *Energy Storage Mater.* **2021**, *43*, 221.
[7] P. Albertus, S. Babinec, S. Litzelman, A. Newman, *Nat. Energy* **2017**, *3*, 16.
[8] J. Duan, Y. Zheng, W. Luo, W. Wu, T. Wang, Y. Xie, S. Li, J. Li, Y. Huang, *Natl. Sci. Rev.* **2020**, *7*, 1208.
[9] J. Wu, X. Li, Z. Rao, X. Xu, Z. Cheng, Y. Liao, L. Yuan, X. Xie, Z. Li, Y. Huang, *Nano Energy* **2020**, *72*, 104725.
[10] X. Zheng, Z. Gu, X. Liu, Z. Wang, J. Wen, X. Wu, W. Luo, Y. Huang, *Energy Environ. Sci.* **2020**, *13*, 1788.
[11] H. Y. Zhang, S. L. Ju, G. L. Xia, D. L. Sun, X. B. Yu, *Adv. Funct. Mater.* **2021**, *31*, 2009712.
[12] W. L. Liu, L. Y. Du, S. L. Ju, X. Y. Cheng, Q. Wu, Z. Hu, X. B. Yu, *ACS Nano* **2021**, *15*, 5679.
[13] W. L. Liu, X. X. Yuan, X. B. Yu, *ACS Appl. Mater. Interfaces* **2021**, *13*, 12016.
[14] T. Jin, X. Ji, P. F. Wang, K. Zhu, J. Zhang, L. Cao, L. Chen, C. Cui, T. Deng, S. Liu, N. Piao, Y. Liu, C. Shen, K. Xie, L. Jiao, C. Wang, *Angew. Chem., Int. Ed.* **2021**, *60*, 11943.
[15] Z. L. Jian, W. Luo, X. L. Ji, *J. Am. Chem. Soc.* **2015**, *137*, 11566.
[16] J. C. Pramudita, D. Sehrawat, D. Goonetilleke, N. Sharma, *Adv. Energy Mater.* **2017**, *7*, 1602911.
[17] T. Zhang, Y. Tang, S. Guo, X. Cao, A. Pan, G. Fang, J. Zhou, S. Liang, *Energy Environ. Sci.* **2020**, *13*, 4625.
[18] F. Wang, L. E. Blanc, Q. Li, A. Faraone, X. Ji, H. H. Chen-Mayer, R. L. Paul, J. A. Dura, E. Hu, K. Xu, L. F. Nazar, C. Wang, *Adv. Energy Mater.* **2021**, *11*, 2102016.
[19] L. Ma, T. P. Pollard, Y. Zhang, M. A. Schroeder, M. S. Ding, A. V. Cresce, R. Sun, D. R. Baker, B. A. Helms, E. J. Maginn, C. Wang, O. Borodin, K. Xu, *Angew. Chem., Int. Ed.* **2021**, *60*, 12438.
[20] W. Sun, F. Wang, B. Zhang, M. Y. Zhang, V. Kupers, X. Ji, C. Theile, P. Bieker, K. Xu, C. S. Wang, M. Winter, *Science* **2021**, *371*, 46.
[21] L. Yao, S. L. Ju, T. Xu, X. B. Yu, *ACS Nano* **2021**, *15*, 13662.
[22] J. N. Zheng, S. L. Ju, L. Yao, G. L. Xia, X. B. Yu, *J. Power Sources* **2021**, *511*, 230450.
[23] G. L. Zhu, G. L. Xia, X. B. Yu, *Small* **2021**, *17*, 2101845.
[24] M. Salama, R. Attias, B. Hirsch, R. Yemini, Y. Gofer, M. Noked, D. Aurbach, *ACS Appl. Mater. Interfaces* **2018**, *10*, 36910.
[25] S. Tan, F. Xiong, J. Wang, Q. An, L. Mai, *Mater. Horiz.* **2020**, *7*, 1971.
[26] J. Wang, S. Tan, G. Zhang, Y. Jiang, Y. Yin, F. Xiong, Q. Li, D. Huang, Q. Zhang, L. Gu, Q. An, L. Mai, *Sci. China Mater.* **2020**, *63*, 1651.
[27] L. W. Gaddum, H. E. French, *J. Am. Chem. Soc.* **1927**, *49*, 1295.
[28] J. H. Connor, W. E. Reid, G. B. Wood, *J. Electrochem. Soc.* **1957**, *104*, 38.
[29] A. Brenner, *J. Electrochem. Soc.* **1971**, *118*, 99.
[30] R. J. H. Thomas, D. Gregory, C. Winterton, *J. Electrochem. Soc.* **1990**, *137*, 3104.

[31] D. Aurbach, Z. Lu, A. Schechter, Y. Gofer, H. Gizbar, R. Turgeman, Y. Cohen, M. Moshkovich, E. Levi, *Nature* **2000**, *407*, 724.
[32] M. Matsui, *J. Power Sources* **2011**, *196*, 7048.
[33] R. E. Doe, R. Han, J. Hwang, A. J. Gmitter, I. Shterenberg, H. D. Yoo, N. Pour, D. Aurbach, *Chem. Commun.* **2014**, *50*, 243.
[34] O. Tutusaus, R. Mohtadi, T. S. Arthur, F. Mizuno, E. G. Nelson, Y. V. Sevryugina, *Angew. Chem., Int. Ed.* **2015**, *54*, 7900.
[35] I. Shterenberg, M. Salama, H. D. Yoo, Y. Gofer, J.-B. Park, Y.-K. Sun, D. Aurbach, *J. Electrochem. Soc.* **2015**, *162*, A7118.
[36] I. Shterenberg, M. Salama, Y. Gofer, D. Aurbach, *Langmuir* **2017**, *33*, 9472.
[37] T. Gao, S. Hou, F. Wang, Z. Ma, X. Li, K. Xu, C. Wang, *Angew. Chem., Int. Ed. Engl.* **2017**, *56*, 13526.
[38] K. A. See, K. W. Chapman, L. Zhu, K. M. Wiaderek, O. J. Borkiewicz, C. J. Barile, P. J. Chupas, A. A. Gewirth, *J. Am. Chem. Soc.* **2016**, *138*, 328.
[39] J. Luo, S. J. He, T. L. Liu, *ACS Energy Lett.* **2017**, *2*, 1197.
[40] R. Mohtadi, O. Tutusaus, T. S. Arthur, Z. Zhao-Karger, M. Fichtner, *Joule* **2021**, *5*, 581.
[41] J. Muldoon, C. B. Bucur, A. G. Oliver, J. Zajicek, G. D. Allred, W. C. Boggess, *Energy Environ. Sci.* **2013**, *6*, 482.
[42] J. Muldoon, C. B. Bucur, A. G. Oliver, T. Sugimoto, M. Matsui, H. S. Kim, G. D. Allred, J. Zajicek, Y. Kotani, *Energy Environ. Sci.* **2012**, *5*, 5941.
[43] L. Zhou, Q. Liu, Z. Zhang, K. Zhang, F. Xiong, S. Tan, Q. An, Y. M. Kang, Z. Zhou, L. Mai, *Adv. Mater.* **2018**, *30*, 1801984.
[44] R. Davidson, A. Verma, D. Santos, F. Hao, C. Fincher, S. Xiang, J. Van Buskirk, K. Xie, M. Pharr, P. P. Mukherjee, S. Banerjee, *ACS Energy Lett.* **2018**, *4*, 375.
[45] Y. Zhan, W. Zhang, B. Lei, H. Liu, W. Li, *Front. Chem.* **2020**, *8*, 125.
[46] P. W. Jaschin, Y. Gao, Y. Li, S. H. Bo, *J. Mater. Chem. A* **2020**, *8*, 2875.
[47] R. Deivanayagam, B. J. Ingram, R. Shahbazian-Yassar, *Energy Storage Mater.* **2019**, *21*, 136.
[48] E. R. Gobechiya, M. V. Sukhanov, V. I. Pet'kov, Y. K. Kabalov, *Crystallogr. Rep.* **2008**, *53*, 53.
[49] S. Ikeda, M. Takahashi, J. Ishikawa, K. Ito, *Solid State Ionics* **1987**, *23*, 125.
[50] K. Nomura, S. Ikeda, K. Ito, H. Einaga, *J. Electroanal. Chem.* **1992**, *326*, 351.
[51] A. Kazakos-Kijowski, S. Komarneni, D. Agrawal, R. Roy, *Mater. Res. Bull.* **1988**, *23*, 1177.
[52] N. K. Anuar, S. B. R. S. Adnan, N. S. Mohamed, *Ceram. Int.* **2014**, *40*, 13719.
[53] M. Adamu, G. M. Kale, *J. Phys. Chem. C* **2016**, *120*, 17909.
[54] B. Liang, V. Keshishian, S. Liu, E. Yi, D. Jia, Y. Zhou, J. Kieffer, B. Ye, R. M. Laine, *Electrochim. Acta* **2018**, *272*, 144.
[55] N. K. Anuar, S. B. R. S. Adnan, M. H. Jaafar, N. S. Mohamed, *Ionics* **2016**, *22*, 1125.
[56] N. K. Anuar, N. S. Mohamed, *J. Sol-Gel Sci. Technol.* **2016**, *80*, 249.
[57] K. Kajihara, H. Nagano, T. Tsujita, H. Munakata, K. Kanamura, *J. Electrochem. Soc.* **2017**, *164*, A2183.
[58] N. Imanaka, Y. Okazaki, G. Adachiz, *Electrochem. Solid-State Lett.* **2000**, *3*, 327.
[59] N. Imanaka, Y. Okazaki, G. Adachi, *Ionics* **2001**, *7*, 440.
[60] S. Tamura, M. Yamane, Y. Hoshino, N. Imanaka, *J. Solid State Chem.* **2016**, *235*, 7.
[61] N. Imanaka, M. Itaya, G. Adachi, *Mater. Lett.* **2002**, *53*, 1.
[62] S. Barth, R. Olazcuaga, P. Gravereau, G. L. Flem, P. Hagenmuller, *Mater. Lett.* **1993**, *16*, 96.
[63] K. Makino, Y. Katayama, T. Miura, T. Kishi, *J. Power Sources* **2001**, *99*, 66.
[64] K. Makino*, Y. Katayama, T. Miura, T. Kishi, *J. Power Sources* **2002**, *112*, 85.
[65] H. Takahashia, H. Takamura, *Key Eng. Mater.* **2012**, *508*, 291.
[66] H. Takahashi, H. Takamura, *Mater. Trans.* **2012**, *53*, 932.
[67] Z. A. Halim, S. B. R. S. Adnan, N. S. Mohamed, *Ceram. Int.* **2016**, *42*, 4452.
[68] Z. A. Halim, S. B. R. S. Adnan, F. M. Salleh, N. S. Mohamed, *J. Magnesium Alloys* **2017**, *5*, 439.
[69] K. Nomura, S. Ikeda, K. Ito, H. Einaga, *Chem. Lett.* **1992**, 1897.
[70] M. Sulaiman, N. Che Su, N. S. Mohamed, *Ionics* **2016**, *23*, 443.
[71] M. Sulaiman, A. A. Rahman, N. S. Mohamed, *Int. J. Electrochem. Sci.* **2013**, *8*, 6647.
[72] N. Imanaka, Y. Okazaki, G.-y. Adachi, *J. Mater. Chem.* **2000**, *10*, 1431.
[73] A. H. Ahmad, F. S. A. Ghani, *AIP Conf. Proc.* **2009**, 1136.
[74] A. Omote, S. Yotsuhashi, Y. Zenitani, Y. Yamada, D. Edwards, *J. Am. Ceram. Soc.* **2011**, *94*, 2285.
[75] J. Su, T. Tsuruoka, T. Tsujita, Y. Nishitani, K. Nakura, K. Terabe, *Chem. Mater.* **2019**, *31*, 5566.
[76] H. W. Li, K. Kikuchi, Y. Nakamori, N. Ohba, K. Miwa, S. Towata, S. Orimo, *Acta Mater.* **2008**, *56*, 1342.
[77] H. W. Li, K. Kikuchi, T. Sato, Y. Nakamori, N. Ohba, M. Aoki, K. Miwa, S. Towata, S. Orimo, *Mater. Trans.* **2008**, *49*, 2224.
[78] G. L. Soloveichik, Y. Gao, J. Rijssenbeek, M. Andrus, S. Kniajanski, R. C. Bowman, S. J. Hwan, J. C. Zhao, *Int. J. Hydrogen Energy* **2009**, *34*, 916.
[79] X. W. Chen, F. Yuan, Q. F. Gu, Y. B. Tan, H. K. Liu, S. X. Dou, X. B. Yu, *Int. J. Hydrogen Energy* **2013**, *38*, 16199.
[80] F. Yuan, X. W. Chen, Q. F. Gu, Z. W. Tang, X. B. Yu, *Int. J. Hydrogen Energy* **2013**, *38*, 5322.
[81] R. Mohtadi, F. Mizuno, *Beilstein J. Nanotechnol.* **2014**, *5*, 1291.
[82] J. H. Connor, W. E. Reid, G. B. Wood, *J. Electrochem. Soc.* **1957**, *104*, 38.
[83] T. D. Gregory, R. J. Hoffman, R. C. Winterton, *J. Electrochem. Soc.* **1990**, *137*, 775.
[84] R. Mohtadi, M. Matsui, T. S. Arthur, S.-J. Hwang, *Angew. Chem., Int. Ed.* **2012**, *51*, 9780.
[85] D. Blanchard, J. B. Maronsson, M. D. Riktor, J. Kheres, D. Sveinbjörnsson, E. Gil Bardají, A. Léon, F. Juranyi, J. Wuttke, K. Lefmann, B. C. Hauback, M. Fichtner, T. Vegge, *J. Phys. Chem. C* **2012**, *116*, 2013.
[86] T. Ikeshoji, E. Tsuchida, S. Takagi, M. Matsuo, S.-i. Orimo, *RSC Adv.* **2014**, *4*, 1366.
[87] M. Matsuo, H. Oguchi, T. Sato, H. Takamura, E. Tsuchida, T. Ikeshoji, S. Orimo, *J. Alloys Compd.* **2013**, *580*, S98.
[88] K. Kisu, S. Kim, M. Inukai, H. Oguchi, S. Takagi, S. Orimo, *ACS Appl. Energy Mater.* **2020**, *3*, 3174.
[89] Y. G. Yan, W. Dononelli, M. Jorgensen, J. B. Grinderslev, Y. S. Lee, Y. W. Cho, R. Cerny, B. Hammer, T. R. Jensen, *Phys. Chem. Chem. Phys.* **2020**, *22*, 9204.
[90] Y. G. Yan, J. B. Grinderslev, M. Jorgensen, L. N. Skov, J. Skibsted, T. R. Jensen, *ACS Appl. Energy Mater.* **2020**, *3*, 9264.
[91] T. F. Zhang, Y. M. Wang, T. Song, H. Miyaoka, K. Shinzato, H. Miyaoka, T. Ichikawa, S. Q. Shi, X. G. Zhang, S. Isobe, N. Hashimoto, Y. Kojima, *Joule* **2018**, *2*, 1522.
[92] T. Noritake, K. Miwa, M. Aoki, M. Matsumoto, S. Towata, H. W. Li, S. Orimo, *Int. J. Hydrogen Energy* **2013**, *38*, 6730.
[93] T. Noritake, K. Miwa, M. Aoki, M. Matsumoto, S. Towata, H. W. Li, S. Orimo, *J. Alloys Compd.* **2013**, *580*, S85.
[94] S. Higashi, K. Miwa, M. Aoki, K. Takechi, *Chem. Commun.* **2014**, *50*, 1320.
[95] M. Abbasnejad, S. J. Azimi, M. R. Mohammadizadeh, *Int. J. Hydrogen Energy* **2018**, *43*, 1587.
[96] R. L.e Ruyet, R. Berthelot, E. Salager, P. Florian, B. Fleutot, R. Janot, *J. Phys. Chem. C* **2019**, *123*, 10756.
[97] R. L.e Ruyet, B. Fleutot, R. Berthelot, Y. Benabed, G. Hautier, Y. Filinchuk, R. Janot, *ACS Appl. Energy Mater.* **2020**, *3*, 6093.

[98] E. Roedern, R. S. Kuhnel, A. Remhof, C. Battaglia, *Sci. Rep.* **2017**, *7*, 46189.
[99] C. C. Liang, *J. Electrochem. Soc.* **1973**, *120*, 1289.
[100] V. Gulino, L. Barberis, P. Ngene, M. Baricco, P. E. de Jongh, *ACS Appl. Energy Mater.* **2020**, *3*, 4941.
[101] T. Burankova, E. Roedern, A. E. Maniadaki, H. Hagemann, D. Rentsch, Z. Lodziana, C. Battaglia, A. Remhof, J. P. Embs, *J. Phys. Chem. Lett.* **2018**, *9*, 6450.
[102] M. Heere, A. L. Hansen, S. Payandeh, N. Aslan, G. Gizer, M. H. Sorby, B. C. Hauback, C. Pistidda, M. Dornheim, W. Lohstroh, *Sci. Rep.* **2020**, *10*, 9080.
[103] Y. Torii, S. Machida, S. Shigematu, in *Proc. 2007 Spring Meeting of Japan Society of Powder and Powder Metallurgy*, Japan **2007**, p. 248.
[104] T. Yamanaka, A. Hayashi, A. Yamauchi, M. Tatsumisago, *Solid State Ionics* **2014**, *262*, 601.
[105] A. Hayashi, K. Noi, A. Sakuda, M. Tatsumisago, *Nat. Commun.* **2012**, *3*, 856.
[106] N. Tanibata, K. Noi, A. Hayashi, M. Tatsumisago, *RSC Adv.* **2014**, *4*, 17120.
[107] L. Zhang, D. Zhang, K. Yang, X. Yan, L. Wang, J. Mi, B. Xu, Y. Li, *Adv. Sci.* **2016**, *3*, 1600089.
[108] L. Zhang, K. Yang, J. Mi, L. Lu, L. Zhao, L. Wang, Y. Li, H. Zeng, *Adv. Energy Mater.* **2015**, *5*, 1501294.
[109] P. Canepa, S. H. Bo, G. Sai Gautam, B. Key, W. D. Richards, T. Shi, Y. Tian, Y. Wang, J. Li, G. Ceder, *Nat. Commun.* **2017**, *8*, 1759.
[110] L. P. Wang, Z. Zhao-Karger, F. Klein, J. Chable, T. Braun, A. R. Schur, C. R. Wang, Y. G. Guo, M. Fichtner, *ChemSusChem* **2019**, *12*, 2286.
[111] H. C. Zhou, J. R. Long, O. M. Yaghi, *Chem. Rev.* **2012**, *112*, 673.
[112] H. Furukawa, K. E. Cordova, M. O'Keeffe, O. M. Yaghi, *Science* **2013**, *341*, 1230444.
[113] N. Stock, S. Biswas, *Chem. Rev.* **2012**, *112*, 933.
[114] R. Zhao, Y. Wu, Z. Liang, L. Gao, W. Xia, Y. Zhao, R. Zou, *Energy Environ. Sci.* **2020**, *13*, 2386.
[115] S. S. Park, Y. Tulchinsky, M. Dinca, *J. Am. Chem. Soc.* **2017**, *139*, 13260.
[116] D. K. Panda, K. Maity, A. Palukoshka, F. Ibrahim, S. Saha, *ACS Sustainable Chem. Eng.* **2019**, *7*, 4619.
[117] B. M. Wiers, M. L. Foo, N. P. Balsara, J. R. Long, *J. Am. Chem. Soc.* **2011**, *133*, 14522.
[118] M. L. Aubrey, R. Ameloot, B. M. Wiers, J. R. Long, *Energy Environ. Sci.* **2014**, *7*, 667.
[119] L. Shen, H. B. Wu, F. Liu, J. L. Brosmer, G. Shen, X. Wang, J. I. Zink, Q. Xiao, M. Cai, G. Wang, Y. Lu, B. Dunn, *Adv. Mater.* **2018**, *30*, 1707476.
[120] M. Dinca, A. Dailly, J. R. Long, *Chemistry* **2008**, *14*, 10280.
[121] E. M. Miner, S. S. Park, M. Dinca, *J. Am. Chem. Soc.* **2019**, *141*, 4422.
[122] H. B. Wu, X. W. Lou, *Sci. Adv.* **2017**, *3*, eaap9252.
[123] B. Park, J. L. Schaefer, *J. Electrochem. Soc.* **2020**, *167*, 070545.
[124] T. F. Zhang, W. J. He, W. Zhang, T. Wang, P. Li, Z. M. Sun, X. B. Yu, *Chem. Sci.* **2020**, *11*, 8686.
[125] L. L. Yang, A. R. McGhie, G. C. Farrington, *J. Electrochem. Soc.* **1986**, *133*, 1380.
[126] L. L. Yang, R. Huq, G. C. Farrington, *Solid State Ionics* **1986**, *18*, 291.
[127] A. Bakker, S. Gejji, J. Lindgren, K. Hermansson, M. M. Probst, *Polymer* **1995**, *36*, 4371.
[128] A. Ab Aziz, Y. Tominaga, *Ionics* **2018**, *24*, 3475.
[129] S. Ramalingaiah, D. S. Reddy, M. J. Reddy, E. Laxminarsaiah, U. V. S. Rao, *Mater. Lett.* **1996**, *29*, 285.
[130] J. L. Acosta, E. Morales, *Electrochim. Acta* **1998**, *43*, 791.
[131] J. Shi, C. A. Vincent, *Solid State Ionics* **1993**, *60*, 11.
[132] C. A. Vincent, *Electrochim. Acta* **1995**, *40*, 2035.
[133] S. K. Jeong, Y. K. Jo, N. J. Jo, *Electrochim. Acta* **2006**, *52*, 1549.
[134] A. R. Polu, R. Kumar, *Chin. J. Polym. Sci.* **2013**, *31*, 641.
[135] S. Ramesh, S.-C. Lu, E. Morris, *J. Taiwan Inst. Chem. Eng.* **2012**, *43*, 806.
[136] L. T. Ma, X. L. Li, G. B. Zhang, Z. D. Huang, C. P. Han, H. F. Li, Z. J. Tang, C. Y. Zhi, *Energy Storage Mater.* **2020**, *31*, 451.
[137] M. Ramaswamy, T. Malayandi, S. Subramanian, J. Srinivasalu, M. Rangaswamy, *Ionics* **2017**, *23*, 1771.
[138] A. B. Puthirath, T. Tsafack, S. Patra, P. Thakur, N. Chakingal, S. K. Saju, A. Baburaj, K. Kato, G. Babu, T. N. Narayanan, P. M. Ajayan, *Phys. Chem. Chem. Phys.* **2020**, *22*, 19108.
[139] A. R. Polu, R. Kumar, *Bull. Mater. Sci.* **2011**, *34*, 1063.
[140] K. M. Anilkumar, B. Jinisha, M. Manoj, S. Jayalekshmi, *Eur. Polym. J.* **2017**, *89*, 249.
[141] R. Manjuladevi, S. Selvasekarapandian, M. Thamilselvan, R. Mangalam, S. Monisha, P. C. Selvin, *Ionics* **2018**, *24*, 3493.
[142] R. Manjuladevi, M. Thamilselvan, S. Selvasekarapandian, R. Mangalam, M. Premalatha, S. Monisha, *Solid State Ionics* **2017**, *308*, 90.
[143] S. Ponmani, M. R. Prabhu, *J. Mater. Sci.: Mater. Electron.* **2018**, *29*, 15086.
[144] R. C. Agrawal, D. K. Sahu, Y. K. Mahipal, R. Ashrafi, *Mater. Chem. Phys.* **2013**, *139*, 410.
[145] A. R. Polu, R. Kumar, K. V. Kumar, N. K. Jyothi, *AIP Conf. Proc.* **2013**, *1512*, 996.
[146] R. Deivanayagam, M. Cheng, M. C. Wang, V. Vasudevan, T. Foroozan, N. V. Medhekar, R. Shahbazian-Yassar, *ACS Appl. Energy Mater.* **2019**, *2*, 7980.
[147] M. A. K. L. Dissanayake, L. R. A. K. Bandara, L. H. Karaliyadda, P. A. R. D. Jayathilaka, R. S. P. Bokalawala, *Solid State Ionics* **2006**, *177*, 343.
[148] J. C. Sun, Y. B. Zou, S. Z. Gao, L. Y. Shao, C. C. Chen, *ACS Appl. Mater. Interfaces* **2020**, *12*, 54711.
[149] Y. Shao, N. N. Rajput, J. Hu, M. Hu, T. Liu, Z. Wei, M. Gu, X. Deng, S. Xu, K. S. Han, J. Wang, Z. Nie, G. Li, K. R. Zavadil, J. Xiao, C. Wang, W. A. Henderson, J.-G. Zhang, Y. Wang, K. T. Mueller, K. Persson, J. Liu, *Nano Energy* **2015**, *12*, 750.
[150] Nidhi, S. P. , R. Kumar, *J. Alloys Compd.* **2019**, *789*, 6.
[151] M. J. Reddy, P. P. Chu, *J. Power Sources* **2002**, *109*, 340.
[152] Z. Chang, Y. Q. Yang, X. W. Wang, M. X. Li, Z. W. Fu, Y. P. Wu, R. Holze, *Sci. Rep.* **2015**, *5*, 11931.
[153] A. A. Aziz, Y. Tominaga, *Polym. J.* **2018**, *51*, 61.
[154] K. Tang, A. Du, S. Dong, Z. Cui, X. Liu, C. Lu, J. Zhao, X. Zhou, G. Cui, *Adv. Mater.* **2020**, *32*, 1904987.
[155] K. Nakano, Y. Noda, N. Tanibata, M. Nakayama, K. Kajihara, K. Kanamura, *RSC Adv.* **2019**, *9*, 12590.
[156] X. Chen, F. Yuan, Q. Gu, X. Yu, *Dalton Trans.* **2013**, *42*, 14365.

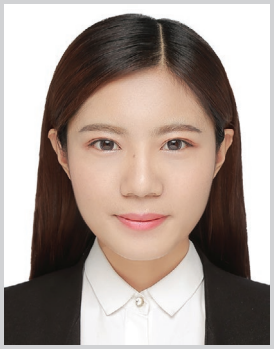

Miao Guo is a research assistant in the Department of Materials Science at Fudan University. She received her M.S. degree in materials science and engineering from General Research Institute for Nonferrous Metals in 2018. Her current research focuses on advanced materials for energy storage devices, such as magnesium-ion batteries and all-solid-state batteries.

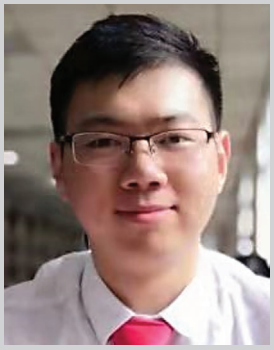

Chongyang Yuan received his BE in polymer material and engineering from Sun Yat-Sen University in 2019. He is currently pursuing his Ph.D. degree under the supervision of Prof. Xuebin Yu in materials physics and chemistry at Fudan University. His current research focuses on nanomaterials for energy storage devices, such as catalytic hydrogen production and all-solid-state batteries.

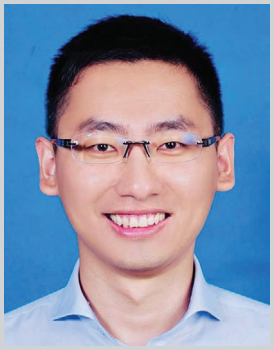

Tengfei Zhang is an associate professor in the College of Materials Science and Technology at Nanjing University of Aeronautics and Astronautics (NUAA). He obtained his BE from the School of Materials Science and Engineering, Central South University, China, and Ph.D. in Advanced Materials from Hokkaido University, Japan. He then worked as a JSPS fellow at Hokkaido University and an assistant professor at Hiroshima University. His current research interests are in the areas of solid-state electrolytes, hydrogen storage materials, and in situ TEM.

Xuebin Yu received his Ph.D. degree from the Shanghai Institute of Microsystem and Information Technology, Chinese Academy of Science in 2004. He then worked as a postdoctoral fellow at the University of Nottingham and the University of Wollongong from January 2005 to December 2006 and March 2007 to March 2008, respectively. In 2008, he joined Fudan University and now works as a professor in the Department of Materials. His research interests cover hydrogen storage, fuel-cell integration with hydrogen systems, hydride-based solid-state electrolytes, lithium/sodium-ion batteries, and preparation of nanomaterials for energy storage.